

¹Tiankuo Jiao²Zekun Li³Zhiyu Zhu

Advanced Control Solutions for DFIG Wind Turbines: From Vector to Predictive Control



Abstract: - This paper investigates advanced control strategies for a doubly-fed induction generator-based wind turbine (DFIG-WT), focusing on vector control and model predictive control (MPC). Initially, it introduces the DFIG-WT structure and general control methods, then explores vector control for effective decoupled power management of active and reactive power. Despite vector control's efficiency, its limitations in handling constraints are highlighted, leading to the adoption of MPC. The study examines MPC's application in current control for three-phase two-level converters, showing its capability for fast tracking and response. Further, it explores MPC's model predictive torque control, demonstrating its proficiency in handling various requirements through a well-designed cost function. Overall, this research emphasizes MPC's adaptability and efficiency in optimizing DFIG-WT performance under varying operational conditions.

Keywords: doubly fed induction generator; vector control; model predictive control; wind turbine control

1 Introduction

This paper explores advanced control strategies for doubly-fed induction generator-based wind turbines (DFIG-WT), highlighting the transition from traditional vector control to the more dynamic model predictive control (MPC). The research begins with a detailed examination of the DFIG-WT, including its structural components and fundamental control mechanisms. A significant focus is placed on vector control and its efficacy in managing active and reactive power through decoupled control. However, recognizing the limitations of vector control in handling constraints, the study introduces MPC as a superior alternative. MPC's adaptability is demonstrated through its application in current control for three-phase two-level converters and its predictive torque control capability. This approach underscores the paper's innovation in optimizing DFIG-WT performance, particularly in managing fast-changing operational conditions and complex power system dynamics.

2 Vector control of doubly fed induction generator-based wind turbine

2.1 Design of vector control

Vector control of the Doubly Fed Induction Generator Wind Turbine (DFIG-WT) is essential due to hardware limitations [3]. The control strategy involves managing torque, active power, and reactive power to optimize wind energy transformation. This section introduces the use of stator flux-oriented vector control for decoupled control of active and reactive power in DFIG-WT. The vector control strategy for the induction generator begins by determining the reference current in the synchronous reference frame using the reference active and reactive power. These reference currents are then used to derive the reference voltages in the dq frame, as the converter controls voltage, not current. The strategy requires transforming reference voltages from the synchronous frame to the actual reference frame and converting real currents in the abc reference frame into currents in the dq reference frame. The vector control scheme applied to the DFIG-WT is detailed in Section 3.1. Additionally, transformations of different reference frames are necessary, with the methodology for frame transformation presented in the final section. For accurate reference frame transformation, the value needs estimation, and a

¹ Affiliation: University of Cambridge, Department of Engineering, Cambridge, CB2 1PZ, United Kingdom
Email: tiankuojiao1@163.com

² Affiliation: University of Edinburgh, School of Engineering, Edinburgh, EH3 9QG, United Kingdom
Email: Sgzli51@163.com

³ Affiliation: Imperial College London, Department of Surgery and Cancer, London, SW7 2AZ, United Kingdom
Email: zhiyuzhu2023@163.com

*Correspondence: Tiankuo Jiao, tiankuojiao1@163.com

phase-locked-loop (PLL) is crucial for synchronization and enhancing robustness [40]. The PLL also assists in rejecting minor disturbances and harmonics [40]. The detailed structure of each module will be further analyzed in subsequent sections.

2.1.2 Current references calculation

Because the stator flux is aligned with the direct axis, then the flux in the q-axis will be zero. Therefore,

$$i_{ds}L_s + i_{dr}L_m = \phi_s \tag{3.1}$$

$$i_{qs}L_s + i_{qr}L_m = 0 \tag{3.2}$$

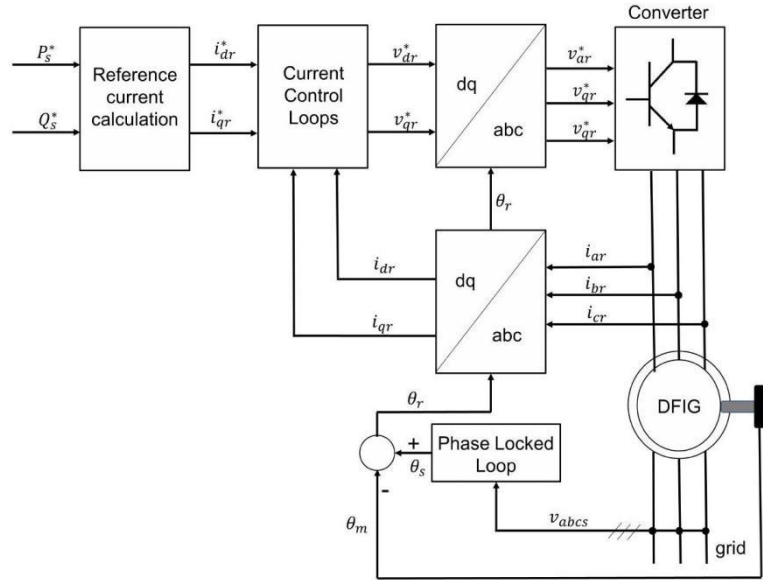


Figure 3.1: The scheme of the vector control applied on DFIG-WT

Then, the stator can be expressed as:

$$i_{ds} = \frac{\phi_s}{L_s} - \frac{L_m}{L_s} i_{dr} \tag{3.3}$$

$$i_{qs} = -\frac{L_m}{L_s} i_{qr} \tag{3.4}$$

Because the flux of stator is dependent on the grid voltage, then:

$$v_{ds} = 0 \tag{3.5}$$

$$v_{qs} = V_g \approx \omega_s \phi_s \tag{3.6}$$

The stator resistor is ignored. When stator flux is in the d-axis, the corresponding voltage can then be assumed to be aligned with the q-axis. Then, the active and reactive power can be expressed by:

$$P_{\text{stator}} = \frac{3}{2} v_{qs} i_{qs} \tag{3.7}$$

$$Q_{\text{stator}} = \frac{3}{2} v_{qs} i_{ds} \tag{3.8}$$

Substitute the above equations into equation 3.7 and 3.8 .

$$P_s = -\frac{3}{2} V_g \frac{L_m}{L_s} i_{qr} \tag{3.9}$$

$$Q_s = \frac{3}{2} V_g \frac{\phi_s}{L_s} - \frac{3}{2} V_g \frac{L_m}{L_s} i_{dr} \tag{3.10}$$

In addition, the reactive power of the stator can also be:

$$Q_s = \frac{3}{2} V_g^2 \frac{1}{\omega_s L_s} - \frac{3}{2} V_g \frac{L_m}{L_s} i_{dr} \quad (3.11)$$

Because the other parameters except the d, q-axis currents are constants, the active power (P) of the stator will only depend on the q-axis current. And the stator reactive power (Q) only relies on the d-axis current. The reference currents can be then expressed by the equations above. Then, the following control loops will be used to obtain the reference voltage. The scheme of the current reference calculation can be seen below 3.2 .

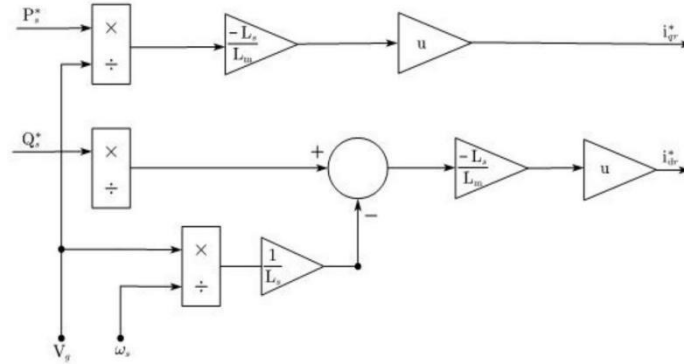


Figure 3.2: The scheme for the calculation of current reference

The control scheme is not completed because the effect of the resistance of the stator is ignored, which leads to the inaccurate reference of active power and reactive power. To solve this problem, the control loops for the active and reactive power are needed. Then, the improved control scheme will be 3.3 .

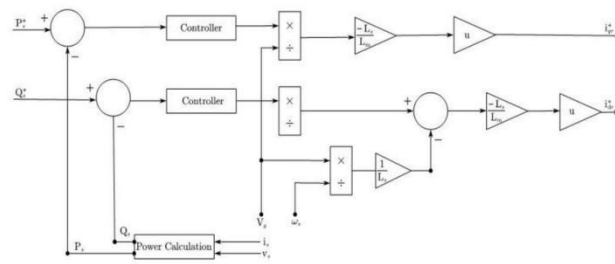


Figure 3.3: The improved scheme for calculating the current reference

The outer power control loops will make reference power more accurate. The resistance of the stator and small disturbances will not lead to inexact power reference. If the torque needs to be adjusted, the equation for the torque, the stator flux and the rotor current is shown in the figure below:

$$T_{em} = \frac{3}{2} p \frac{L_m}{L_s} (\phi_{qs} i_{dr} - \phi_{ds} i_{qr}) \quad (3.12)$$

Because the d axis is aligned with the rotor flux, the torque can be calculated by:

$$T_{em} = \frac{3}{2} p \frac{L_m}{L_s} - \phi_{ds} i_{qr} \quad (3.13)$$

Substitute the equation 3.6 to equation 3.13

$$T_{em} = -\frac{3}{2} p \frac{L_m V_g}{L_s \omega_s} i_{qr} \quad (3.14)$$

Therefore, the torque can be adjusted by the q-axis current because other parameters are constants. Then, the mechanical power is expressed through the torque, then:

$$P_{mec} = -\frac{3}{2}p \frac{L_m V_g}{L_s \omega_s} i_{qr} \omega_m \quad (3.15)$$

Because the relationship between the ω_s and ω_m is:

$$\omega_m = (1 - s)\omega_s \quad (3.16)$$

Substitute the equation 3.16 to the equation 3.15 .

$$P_{mec} = -\frac{3}{2}p \frac{L_m V_g}{L_s} i_{qr} (1 - s) \quad (3.17)$$

Then, the relationship between the mechanical power and stator power will be:

$$P_{mec} = (1 - s)P_s \quad (3.18)$$

2.1.3 Current control loop

Because the converter can only fix the voltage not the current, the reference currents need to be changed to reference voltages. The current control loops will then be needed. In addition, the real currents need to track the currents reference in the synchronous reference frame. That is because variables will be constant in steady state using dq frame. The PI controller is chosen because of its simplicity. The rotor voltage can be expressed as:

$$v_{dr} = R_r i_{dr} - \omega_r \phi_{qr} + \frac{d\phi_{dr}}{dt} \quad (3.19)$$

$$v_{qr} = R_r i_{qr} + \omega_r \phi_{dr} + \frac{d\phi_{qr}}{dt} \quad (3.20)$$

The rotor flux can be obtained as:

$$\phi_{dr} = \left(L_r - \frac{L_m^2}{L_s} \right) i_{dr} + \frac{L_m}{L_s} \phi_{ds} \quad (3.21)$$

$$\phi_{dr} = \left(L_r - \frac{L_m^2}{L_s} \right) i_{qr} \quad (3.22)$$

Then, the rotor voltage can be expressed as:

$$v_{dr} = R_r i_{dr} - L_r \left(\omega_r \sigma i_{qr} + \sigma \frac{di_{dr}}{dt} \right) + \frac{L_m}{L_s} \frac{d\phi_{ds}}{dt} \quad (3.23)$$

$$v_{qr} = R_r i_{qr} - L_r \left(\omega_r \sigma i_{dr} + \sigma \frac{di_{qr}}{dt} \right) + \frac{L_m}{L_s} \phi_{ds} \omega_r \quad (3.24)$$

Where the σ is the leakage coefficient, which can be calculated as:

$$\left(L_r - \frac{L_m^2}{L_s} \right) = L_{\sigma r} + L_m // L_{\sigma s} = \sigma L_r \quad (3.25)$$

The derivative of the flux will be 0 because the voltage will not change in the steady state. Therefore, the last term v_{dr} will disappear. Because the flux of the rotor can also be represented by (From equation 2.64):

$$\vec{\phi}_{dr}^a = L_m \vec{i}_{ds}^a + L_r \vec{i}_{dr}^a \quad (3.26)$$

$$\vec{\phi}_{qr}^a = L_m \vec{i}_{qs}^a + L_r \vec{i}_{qr}^a \quad (3.27)$$

Then, the voltage of the rotor in synchronous dq frame can also be:

$$v_{dr} = R_r i_{dr} - \omega_r (L_m \vec{i}_{qs}^a + L_r \vec{i}_{qr}^a) + \frac{d\phi_{dr}}{dt} \quad (3.28)$$

$$v_{qr} = R_r i_{qr} + \omega_r (L_m \vec{i}_{ds}^a + L_r \vec{i}_{dr}^a) + \frac{d\phi_{qr}}{dt} \quad (3.29)$$

Through obtaining the equations for the rotor voltage, the reference currents will be converted to the reference voltage.

2.2 Simulation results

The principle of stator flux-oriented vector control is explained. In the simulation, the dq model of the DFIG will be implemented. The 9MW wind farm containing 61.5MW wind turbines will be simulated. The wind turbines will connect to the 25KV distribution system and output to the 120kV grid.

2.2.1 Wind turbine

The variable pitch angle wind turbine is used in the simulation. For simplicity, per-unit (pu) system is employed in the wind turbine. The value in pu system can be expressed as:

$$\text{Value expressed in pu} = \frac{\text{Value expressed in normal unit (SI unit)}}{\text{Base value}} \tag{3.30}$$

Generally, the system will choose the nominal value of the system as the base value. In the wind turbine module, the nominal mechanical power is chosen to 9MW and the base power of the generator is chosen to 8MW. The base wind is set to 12 m/s(1pu) with 0.73pu/mechanical power. The rotating speed for the base wind is 1.2 pu. The output power can be calculated by:

$$P_m = C_p \frac{\rho A}{2} * v_{wind}^3 \tag{3.31}$$

Where P_m is the mechanical power, C_p is the performance coefficient, ρ is the air density and A is the area of wind turbine. Because pu system is used in the model, the mechanical power will be changed to:

$$P_{m_{pu}} = k_p C_{p_{pu}} v_{wind}^3 \tag{3.32}$$

Where P_m is the mechanical power in pu system, $C_{p_{pu}}$ is the power coefficient in pu system and $v_{wind_{pu}}$ is the wind speed in pu system. Specially, k_p is the power gain when $C_{p_{pu}}=1pu$ and $v_{wind_{pu}} = 1pu$. Therefore, the wind turbine for simulation can be seen below 3.4

Therefore, the inputs will be the speed of the generator, wind speed and pitch angle in SI system. The value of the λ_{pu} can be obtained by the division of the rotating speed and the speed of wind in pu. After obtaining the real λ , the value of power coefficient will be calculated. After getting the nominal power coefficient, the power coefficient in pu can be obtained. Then, the value of $P_{m_{pu}}$ will be obtained. In the simulation, the simulation time is chosen from 0 – 50 s and the wind speed is set to vary from 8 m/s to 16 m/s at 10 second. The simulation results can be seen below 3.5 .

The mechanical power will vary from -0.2 pu to -0.7pu when the wind speed changes. The control of the pitch angle will be analyzed in the following section.

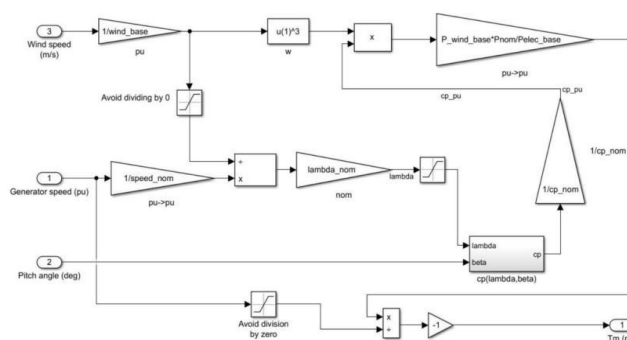


Figure 3.4: Variable pitch angle Wind turbine

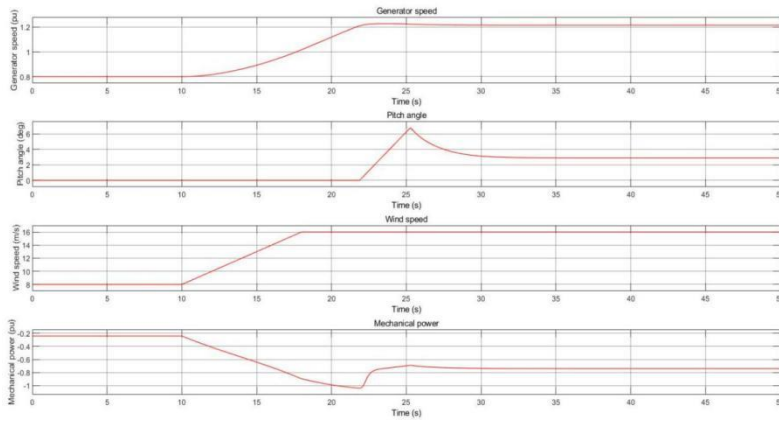


Figure 3.5: Simulation result for the wind turbine

2.2.2 Pitch angle control

As presented in the control scheme 2.8, the pitch angle will vary for high wind speed. The P controller is chosen, and the value of K_p is 500 . The maximum pitch angle is 45 degrees and the slew rate is 2 degree/s. For different wind speeds, the simulation results can be seen below 3.6.

The pitch angle will remain zero degree when the wind speed is low (8 m/s). When the speed of wind changes from low wind speed: 8 m/s to high wind speed: 16 m/s, the simulation results will be 3.7

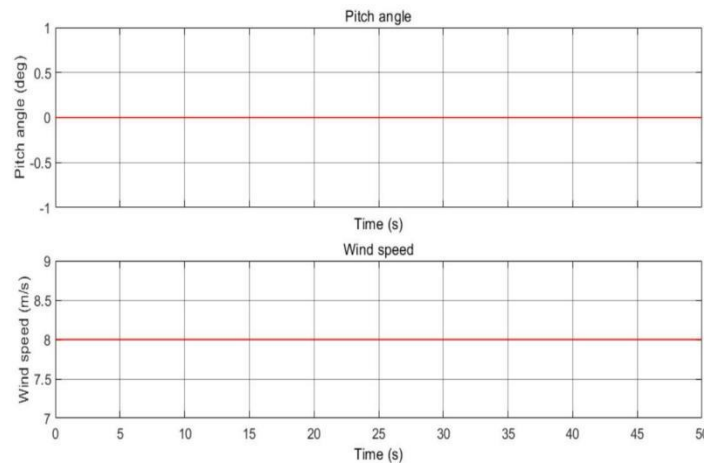


Figure 3.6: Simulation result for the pitch angle control in low wind speed

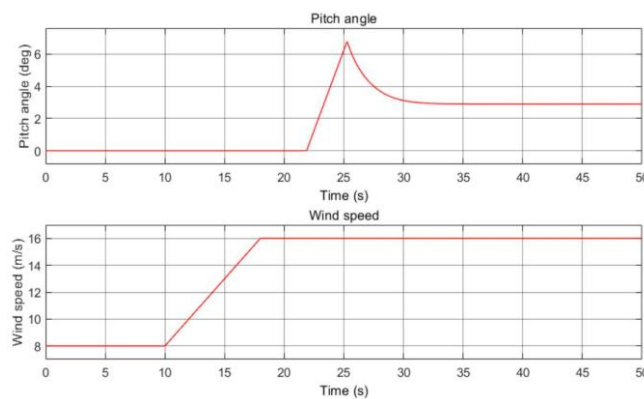


Figure 3.7: Simulation result for controlling the pitch angle when the speed changes

Similarly, the pitch angle will remain 0 degree for low wind speed, but when the speed is greater than the speed of wind (12.1 m/s), the pitch angle will increase to restrict the mechanical output. When the wind speed remains at 16 m/s, the pitch angle will remain at 3 degrees.

2.2.3 Reactive power reference control

The reactive power always needs to be adjusted to be OVAR to improve the system efficiency. However, the reactive power (Q) sometimes is required to remain at the special voltage level to deliver the active power using the transmission line [41]. In addition, the motor load may require reactive power to transform the electronic flow into work. Moreover, voltage sags down may happen if the reactive power is not enough. Therefore, the reactive power will be controlled to OVAR and 3VAR according to the [41] to test the behaviours of the vector control. The PI controller is applied to control the reactive power. The scheme of control realization is: 3.8 .

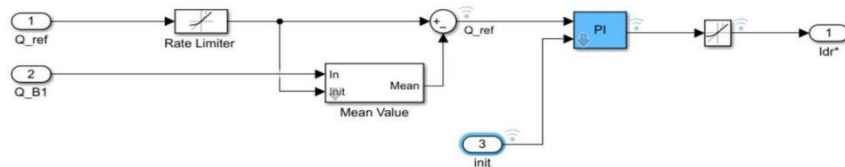


Figure 3.8: Reactive power (Q) control

The value of K_p is set to 0.05 and K_i is set to 5 . To simulate the real situation, the wind speed will vary from 8 m/s to 16 m/s. The simulation time is also set to 50 s. First, the reference reactive power is controlled to be 0 VAR, real reactive power needs to follow the reference power. Then, the simulation results will be 3.9 .

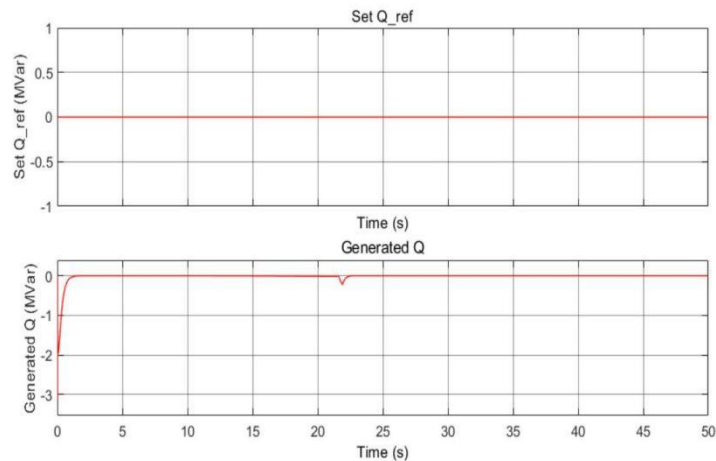


Figure 3.9: Simulation results for 0MVar reference reactive power

The real reactive power follows the reference reactive power quickly and remains 0MVar at steady state. The initial d-axis current of the rotor and reference d-axis current can be seen below 3.10 .

Because the wind changes when the time is 10 seconds, the initial current i_{dr} will also change from that time. Therefore, the reference current will also change from that time. After 25 s, the reference current will not change and remain 0.42pu. Then, the reactive power will be controlled to 3MVAR. The simulation conditions are all the same as the previous control except that the Q is controlled to 3MVar.

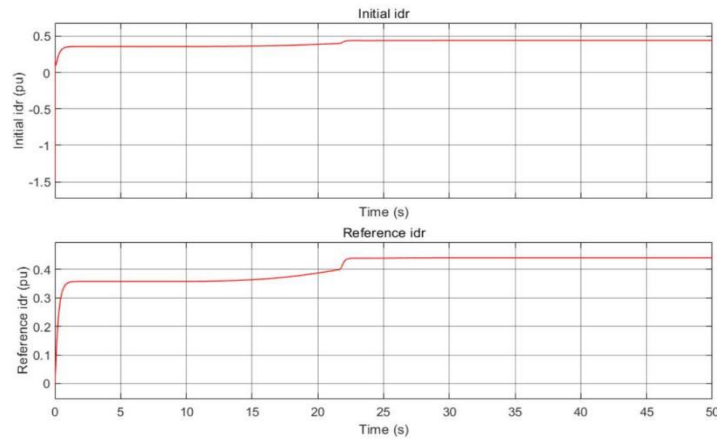


Figure 3.10: Initial d-axis current and reference d-axis current for 0MVar reactive power

The simulation results can be seen below 3.11:

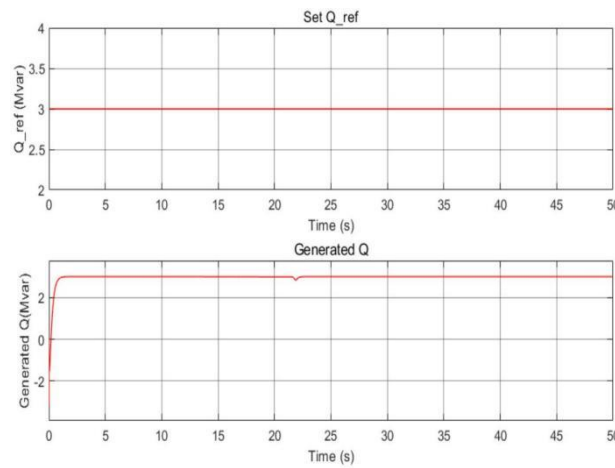


Figure 3.11: Simulation results for 3MVar reference reactive power

The results 3.11 means that the reactive power (Q) can be controlled to a different value also with fast dynamics. Similarly, the simulation results for the d-axis currents are shown below 3.12 .

The reference d-axis current will remain approximately 0.67 pu before the wind changes. And it will increase to 0.73 pu after the wind speed changes to 16 m/s.

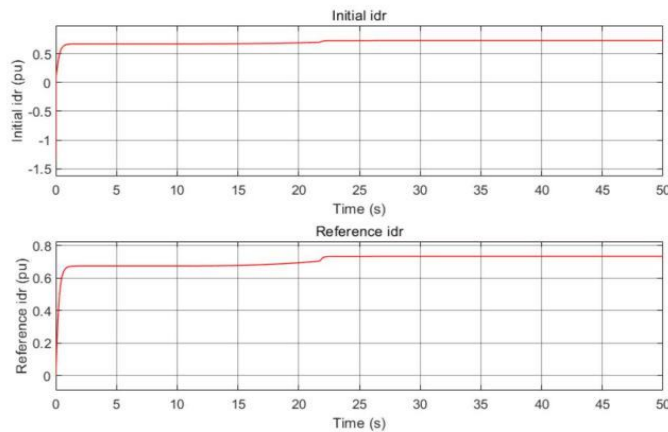


Figure 3.12: Initial d-axis current and reference d-axis current for 3MVar reactive power

2.2.4 Active power reference control

To achieve the active power control, the power point tracking (PPT) needs to be implemented. The power is adjusted to track a defined turbine output power-turbine speed characteristic. The characteristic is explained using the mechanical power characteristics of the turbine by superimposing the ABCD curve for varying wind speeds. The tracking characteristic is given below 3.13

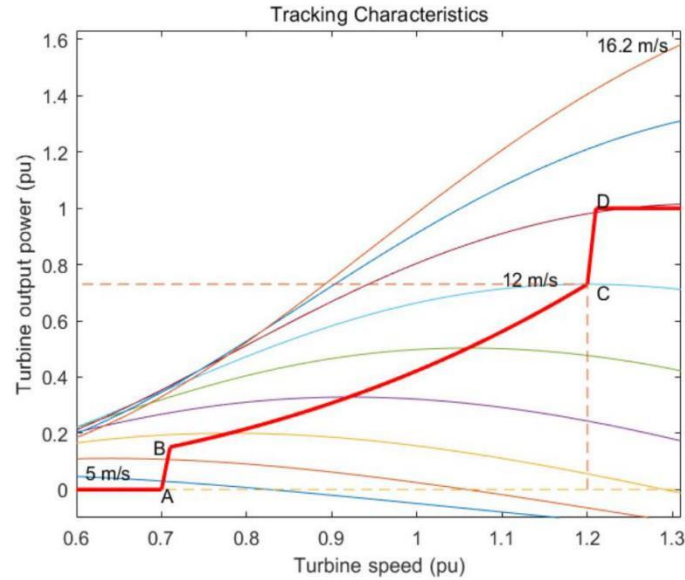


Figure 3.13: Turbine and tracking characteristic

The rotating speed ω_r will be measured and the tracking characteristic is defined as four points. When the speed of turbine is smaller than the speed in point A, the reference power will be 0. When the speed is between the speed in point A and point B, the reference characteristic will be the direct line, and the slope can be calculated. For the point B to point C part, the tracking characteristic needs to realize the maximum power point following. The method implemented in this project is the Optimal power (OP) strategy. When the turbine speed is between the speed in point C and D, the reference characteristic will also be a straight line and the slope can be calculated. For high turbine speed ($> V_D$), the power will remain at 1pu, and the pitch angle control will be used. After setting 0 output power for the speed lower than the speed in point A, and nominal output power for the speed higher than the point in point D. The realization of tracking characteristics from point A to D in Simulink can be seen below:

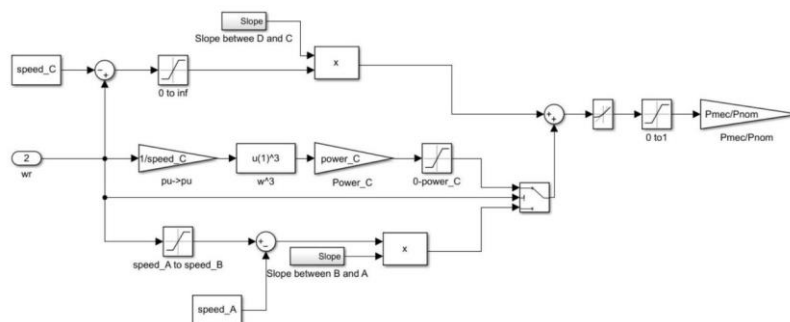


Figure 3.14: Tracking Characteristics from point B to D

In the simulation, the speed at point C is 12 m/s with 0.73 pu output power. The tracking characteristic speed of point A is 0.7pu, 0.71 for point B, 1.2 pu for point C and 1.21pu for point D. There are three branches for different turbine speeds. When the turbine speed is between points C and D, the first branch will be used. The method of calculating the slop between point D and point C can be seen below:

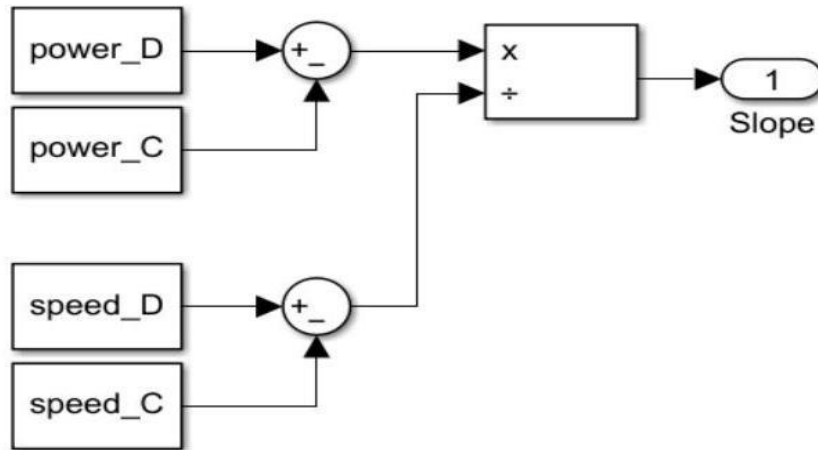


Figure 3.15: The calculation of the slope between points D and C

For point C to point D part, the slope will be calculated by the division between the difference of the powers and the difference between the speeds. The limiter will make sure the first branch will be used only if the turbine speed is larger than that in point C.

The Optimal power (OP) is achieved in the second branch. Because the power and the speed in point C are defined, the value of the K_{opt} can be known. Then, the power between points B and C can be calculated by multiplying ω_m^3 . The maximum power output in this branch is power C, therefore, the limiter will be needed to limit the maximum power.

For point A to B track (third branch), similarly, the slope between point A and B can be calculated by the division between the difference of the powers and the difference between the speeds.

The switch is used to choose which branch. When the turbine speed is larger than the speed in point B, the second branch will be chosen. And when the turbine speed is lower than that in point B, the third branch will be chosen.

After obtaining the reference power in pu system, the reference power needs to be changed to SI unit. Then, the P_{mec}/P_{nom} gain will be needed. The simulation results for the calculation of the active power (P) can be seen below 3.16

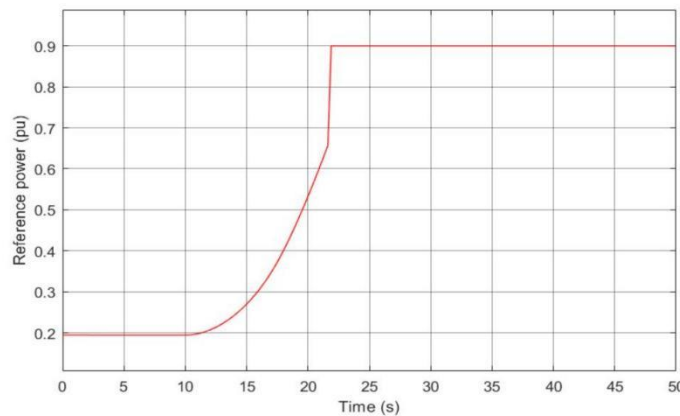


Figure 3.16: The calculation of the reference active power (Ignored the power losses)

The reference active power tracks the maximum power point from point B to C, which means that the maximum power point tracking (MPPT) is achieved. To obtain more accurate reference power, the losses of power are also considered. The losses of the power are calculated by 3.17,

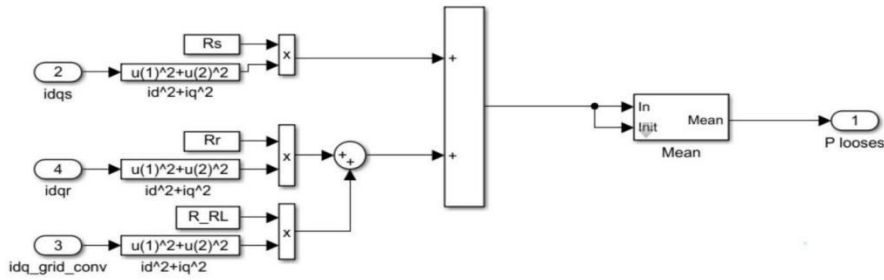


Figure 3.17: The calculation of power losses

Although the power losses in resistors are small, the power is still added to obtain the final reference active power. The small losses of resistors prove the validity of the previous assumptions. Therefore, the power losses in the resistor are usually omitted when obtaining the reference active power. For rigorous experimental results, after adding the power losses, the accurate reference active power can be seen below 3.19 :

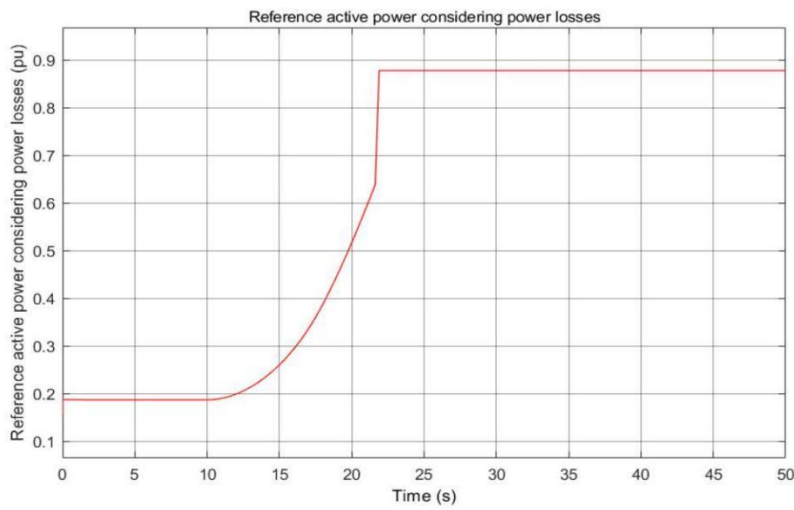


Figure 3.19: The simulation results for reference active power (Considering the power losses)

Therefore, the real reference active power will be less than the active power that ignores the resistor losses. After obtaining the reference active power, the PI control will be employed to obtain the reference q-axis current. The realization of active power control will be 3.20 .

The value of K_p is chosen to 1 and the value of K_i is set to 100 . The simulation results for reference q-axis current i_{qr}^* is shown below 3.21 .

Because the wind changes from 8 m/s to 16 m/s at 10 second, the reference q-axis current will increase from 10 second and be approximately 0.7 pu after 20 second.

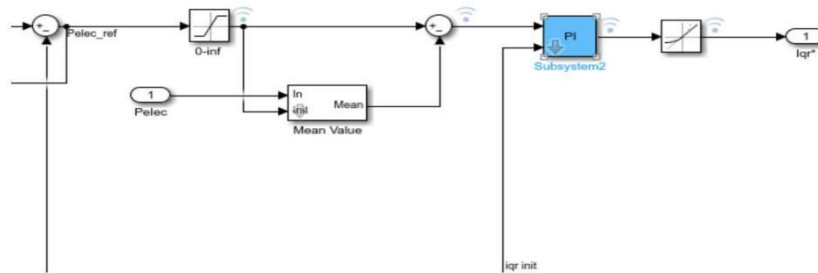


Figure 3.20: The realization of the active power control

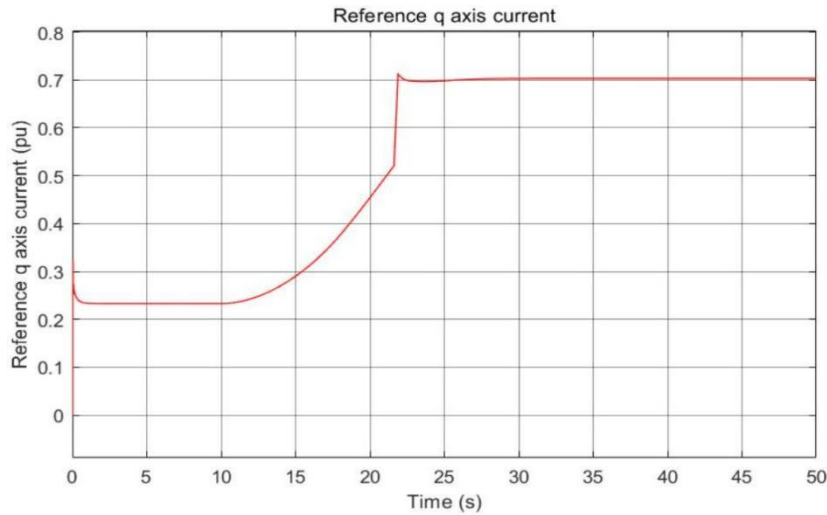


Figure 3.21: The simulation results for reference q axis current i_{qr}^*

2.2.5 Current regulator

After obtaining the reference q and d -axis currents, the currents will change to the reference voltages. The reference voltages can be calculated by:

$$v_{dr} = R_r i_{dr} - \omega_r (L_m \overline{i_{qs}} + L_r \overline{i_{qr}}) + \frac{d\phi_{dr}}{dt} \tag{3.33}$$

$$v_{qr} = R_r i_{qr} + \omega_r (L_m \overline{i_{ds}} + L_r \overline{i_{dr}}) + \frac{d\phi_{qr}}{dt} \tag{3.34}$$

Therefore, the realization in Simulink will be completed by the equations. The realization can be seen below 3.22 :

The reference voltage of d -axis v_d^* , the reference d -axis current i_d^* and real d axis current i_d will enter in the PI controller. The value of K_i is set to 8 and K_p is set to 0.3 . Then, the other terms will be added together to obtain the reference d -axis voltage.

For reference q -axis voltage v_q^* , the control strategy is similar. The reference q -axis current i_q^* and real q -axis current i_q will also enter in the PI controller with remain the same value of K_p and K_i . Then,

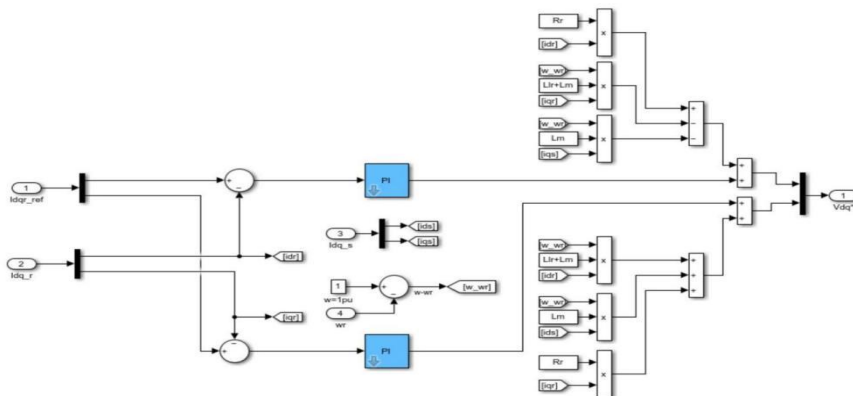


Figure 3.22: The design of the current regulator the other terms will be added together to get the reference voltage of q -axis. After obtaining two axis voltages, they will be combined together to obtain the reference voltage v_{dq}^* . The simulation results for the reference voltage v_{dq}^* is seen below 3.23

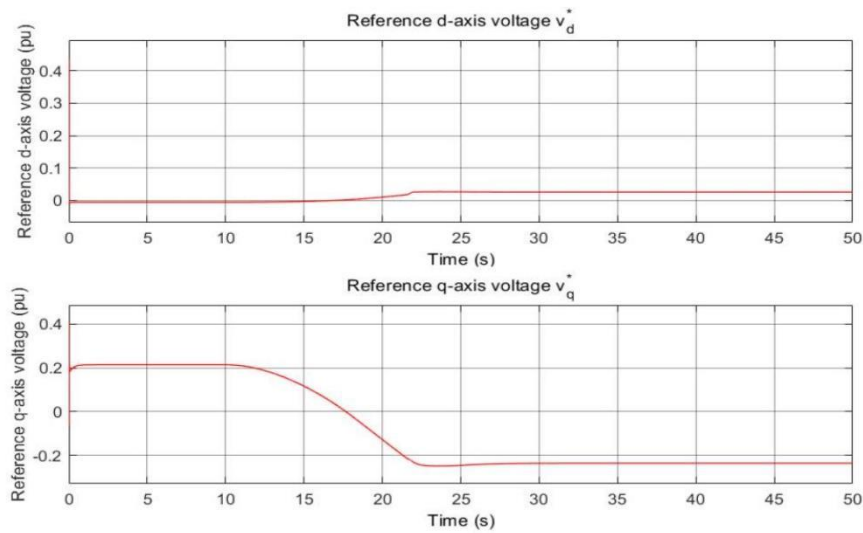


Figure 3.23: The simulation results for the reference voltage

Because the reference reactive power is adjusted to be 0 VAR, the reference *d*-axis voltage will also be controlled near 0 pu.

2.2.6 Converter voltage generation

To obtain 1 pu generated voltage by the converter, the modulation index can be calculated below:

$$m = V_{nom} * 2 * \sqrt{\frac{2}{3}} / V_{dc} \tag{3.35}$$

Where V_{nom} is the RMS value of nominal voltage (phase-to-phase). The realization of the converter voltage generation can be seen below:

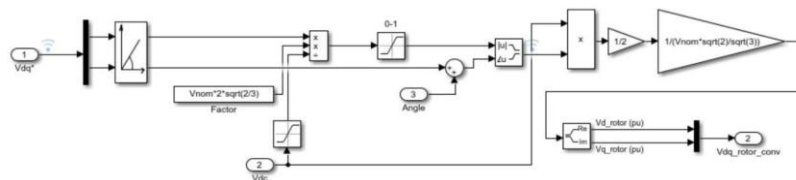


Figure 3.24: The scheme of generating converter voltage

The "0-1" saturation is used to limit the modulation index from 0 to 1 . To obtain the converter voltage in pu system, the rightmost gain will be used. The simulation results for the converter voltage are shown below 3.25 .

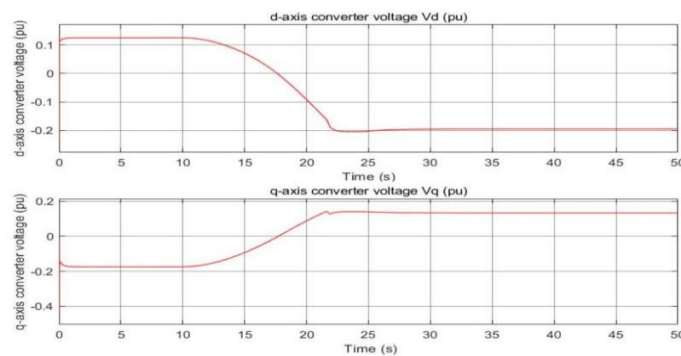


Figure 3.25: The simulation results of converter voltage

The d-axis converter voltage first remains 0.1pu and drops to -0.2pu because of the varies in wind speed. On the contrary, the q-axis converter voltage first remains about -0.19pu and then increases to 0.18pu after the wind speed changes.

2.2.7 Decoupled power control

Because the reactive power control has been implemented and proved to control the reactive power to a non-zero value. Therefore, in the next simulations, the reactive power is still designed to be controlled at 0MVar for convenience. In the previous simulations, the wind speed is designed to vary from 8 m/s to 16 m/s, therefore in this simulation, the performance of the turbine will be tested under different wind speed conditions.

1. Low wind speed 5 m/s

The simulation time is still set to 50 s and the speed of wind is set to 5 m/s, which represents the low wind speed. The simulation results are presented below 3.26 .

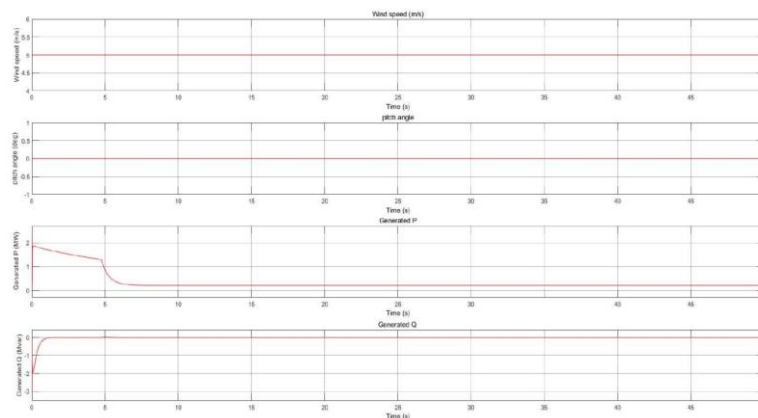


Figure 3.26: The simulation results for wind speed: 5 m/s

Therefore, the active power will be 0MW after 8 s because of low wind speed and the turbine will not generate mechanical power. The reactive power always needs to be controlled to be 0 VAR. In addition, the pitch angle will be 0 degree because the wind speed is too low.

2. Middle wind speed (10 m/s)

The active power will increase because 10 m/s is larger than the speed in point B and the reactive power is controlled to 0 Var. The simulation results can be seen below 3.27.

Similarly, the pitch angle will not change because 10 m/s is still less than the speed in point D and the active power will remain 3.6MW in steady state.

3. High wind speed 14 m/s

Because the wind speed is larger than the speed in point D, the pitch angle control will be used to limit the maximum output power. In addition, the active power (Q) will remain the maximum power in steady state. The simulation results for high wind speed are shown below 3.28 .

The active power will remain 9MW in steady state and the reactive power will still be adjusted to 0 Var. The pitch angle will increase to 0.78 degrees to limit the output power.

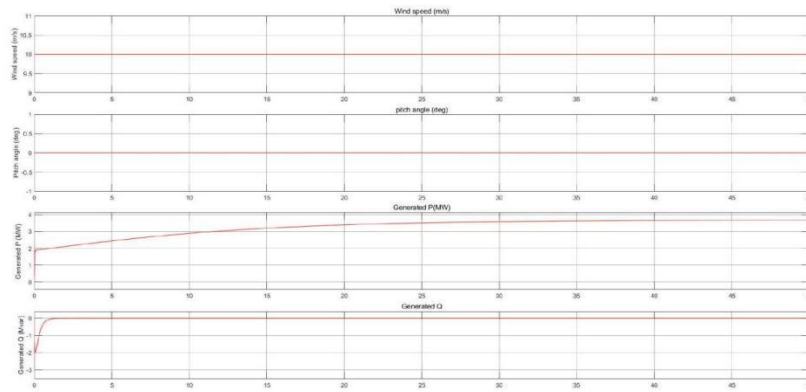


Figure 3.27: The simulation results for wind speed: 10 m/s

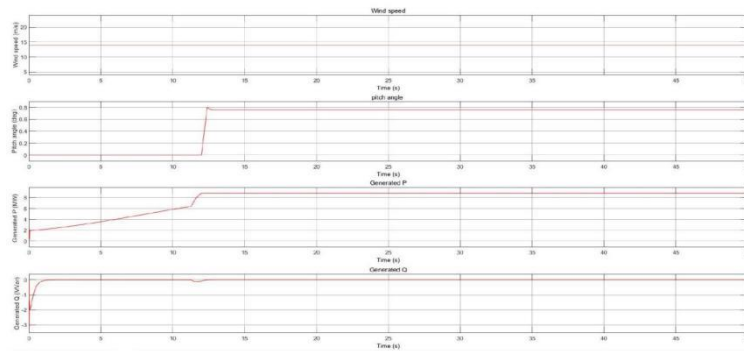
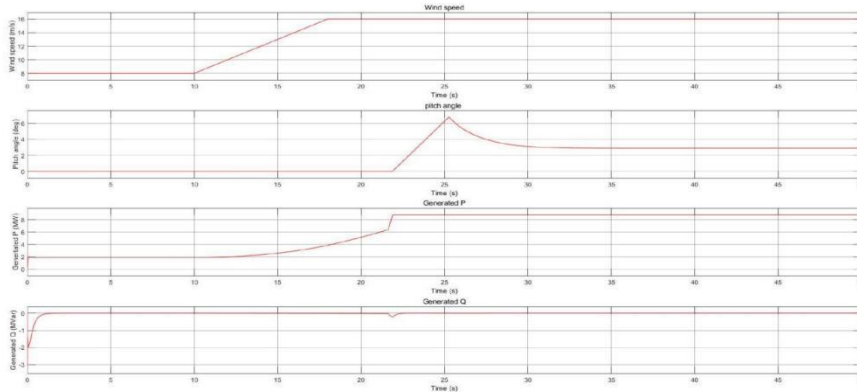


Figure 3.28: The simulation results for wind speed: 14 m/s

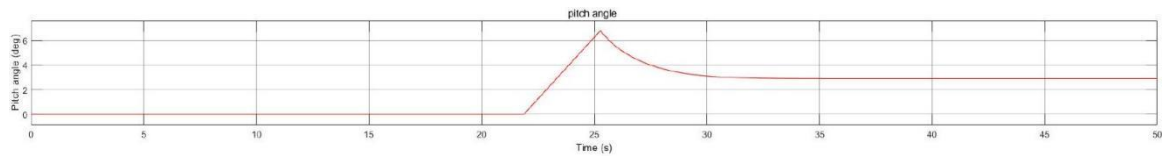
4. Variable wind speed (8 – 16 m/s)

To test the behaviours of the vector control in real life, the wind speed is simulated to change from 8 m/s to 16 m/s. The simulation results can be seen below 3.29 .

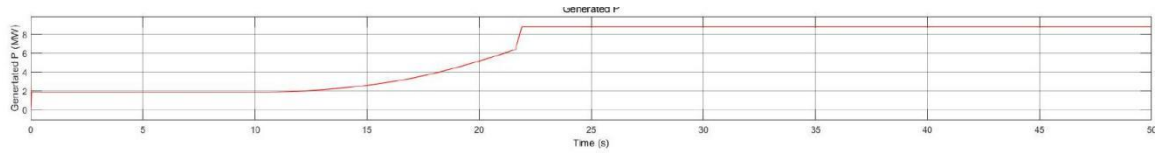
The maximum power point following using the Optimal power (OP) method is achieved. Similarly, the active power needs to be adjusted to 9MW for high wind speed.



Time (s)
pitch angle



Generated P



Generated Q

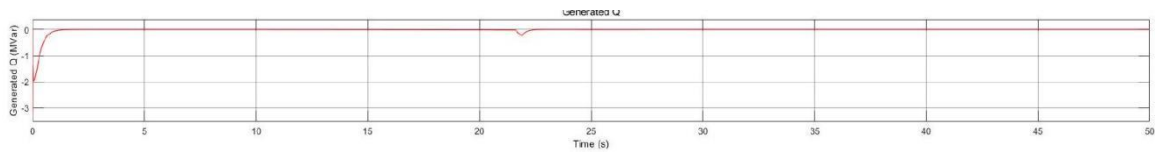


Figure 3.29: The simulation results for wind speed: 8 – 16 m/s

3 Model predictive control (MPC) of doubly fed induction generatorbased wind turbine

This section will first introduce the working principle of model predictive control and then the method of applying model predictive control to power electronics and generators will be explained. Finally, the general model predictive control scheme will be given.

3.1 Working principle of model predictive control

After applying the vector control strategy on the DFIG, the model predictive control can also be used to improve performance. Model predictive control is not the specific control strategy, it involves many kinds of controllers [42]. However, the common elements are that the model of the system will be applied to forecast future behaviours for the variables under a defined time. The designed cost function represents the needed behaviour. And the optimal action that minimizes the value of the cost function will be chosen. Usually, the model used in model predictive control will be the discrete-time model and it can be expressed by the state space model:

$$x(k + 1) = A * x(k) + B * u(k) \tag{4.1}$$

$$y(k) = C * x(k) + D * u(k) \tag{4.2}$$

The state space model is chosen because the derivation of the designed controller will be simple for the multivariable system. The cost function can be expressed as:

$$g = f(x(k), u(k), u(k + 1), \dots u(k + N)) \tag{4.3}$$

The designed cost function needs to consider system limitations, desired behaviours, future states. Because the model predictive control strategy can obtain several optimal actuation for a defined horizon in time, the designed controller only uses the first term in following equation:

$$u(k) = [1 \ 0 \ \dots \ 0] \operatorname{argmin}_u g \tag{4.4}$$

Therefore, the optimization process will repeat again for the next sampling instant using new measured information. The successive sequence of the optimal action will be obtained every time. Therefore, the working principle of MPC is shown below 4.1

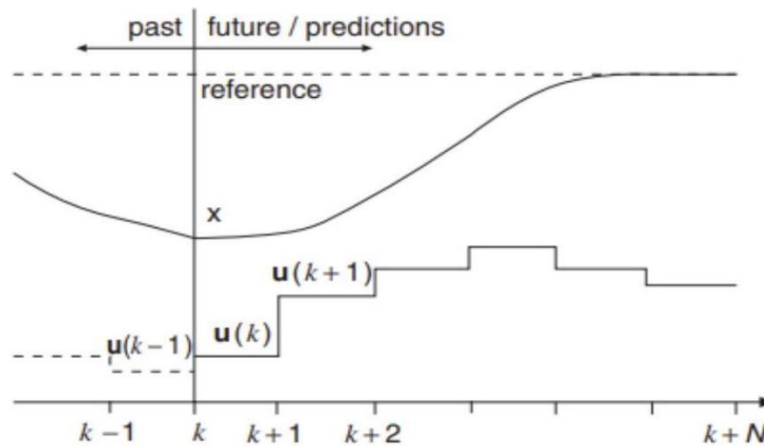


Figure 4.1: The working principle of model predictive control

The future behaviours of the model will be forecast under a defined time $k + N$. The prediction will only rely on the information and data obtained before time k . Then, the designed cost function will be applied to get the sequence of optimal action. But the controller only uses the first actuation, and whole process will repeat again in time $k + 1, k + 2, k + 3, k + 4 \dots k + N$ using new data. To implement the strategy, the basic structure of model predictive control can be seen below:

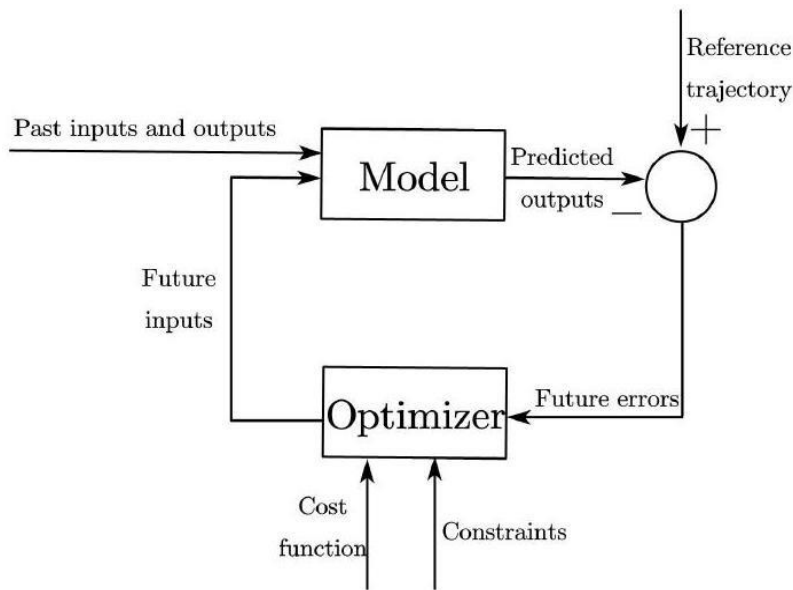


Figure 4.2: The structure of model predictive control

The model used to forecast future outputs incorporates known information, along with the cost function and related constraints, to determine future inputs. This chosen model must effectively capture the dynamics of the process for accurate prediction of future behaviors. With the advancement of microcontrollers, rapid sampling times are achievable, enabling power electronics and generators to utilize model predictive control (MPC) for enhanced performance. After addressing the limitations and constraints, explicit MPC is proposed [8]. This strategy approximates the model of power electronics or drives as a linear system through the modulator [8], simplifying the optimization process. However, the discrete characteristics of power electronics are not considered in explicit MPC [8]. Consequently, the finite control set MPC is developed to fully account for these discrete characteristics. Optimal actuation is calculated through online evaluation of the switching states. The steps required to implement MPC include modeling the converter, identifying the switching states, and clarifying the corresponding voltages and currents for each state. Additionally, an accurate cost function representing the desired behaviors and a discrete-time model to forecast future changes in controlled variables are necessary. For basic converters, the

known switching states are typically limited to on and off. Generally, the number of switching states for a converter can be calculated by:

$$N = x^y \tag{4.5}$$

Where N represents the number of switching states, x represents the number of states and y represents the number of phases. For example, for a 3-phase, 3-level converter, the switching states will be $3^3 = 27$. For the 3-phase 2-level converter, the switching states are $2^3 = 8$. The switching states and related voltage vectors for the three-phase, two-level converter are shown in Figure 2.19 From the figure, 2 or more switching states have the same vector of voltage.

Different control objectives for various strategies are encapsulated within the designed cost function. For instance, the cost function may be adjusted based on the error between measured and predicted data, selecting the optimal actuation that minimizes this value. The strength of model predictive control (MPC) lies in its ability to satisfy diverse requirements by employing a reasonable cost function, with each requirement's weight defined to more effectively meet demands. The selection of controlled variables requires careful consideration, and both measured and predicted variables need to be clearly defined. The discretization method is employed to obtain the discrete model, typically using the Euler forward method, as illustrated below:

$$\frac{dx}{dt} = \frac{x(k+1) - x(k)}{T_{\text{sampling}}} \tag{4.6}$$

Where T_{sampling} is the sampling period. The method can only be used for low-order systems because the error for the high-order system will be large [8]. Because the process of calculating and evaluating the cost function needs time, there is a limitation to the sampling time. Meanwhile, the time becomes long for the converters with more phases and levels because the cost function needs to be evaluated for every switching state. The general control scheme of power converter using model predictive control can be seen below 4.3 .

The variable $x(k)$ will be measured from the load and the predictive model will generate the predicted values. Then, the designed cost function will be employed to compare the difference between the reference $x(k)^*$ and the predicted $x(k+1)$. Then, the control signal will be generated to the converter.

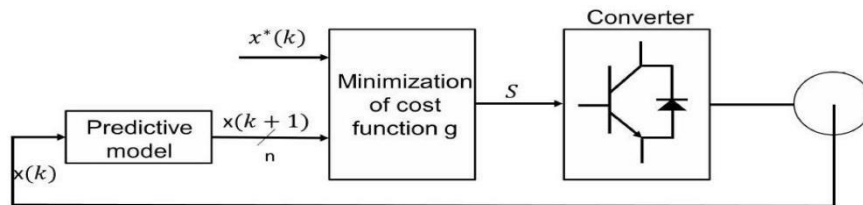


Figure 4.3: The control scheme of the MPC applied on the power converters

3.2 Model predictive current control of the three-phase converter

In this section, the model predictive current control (MPCC) of the converter will be analyzed. The converter with three phases and two levels will be applied to realize the control strategy. First, the control scheme for the converter will be constructed with a reasonable cost function. Then, the converter, load and discrete model will be designed. Finally, the simulation results for model predictive control of the three-phase two-level converter will be conducted.

3.2.1 Cost function and control scheme design

As mentioned above, the realization in model predictive control needs the cost function representing the desired behaviours of the model. For the model predictive current control (MPCC), the currents will be chosen. Because the reference frame is $\alpha\beta$, the cost function can be calculated as:

$$g_{\text{cost}} = |i_{\alpha}^*(k+1) - i_{\alpha}^p(k+1)| + |i_{\beta}^*(k+1) - i_{\beta}^p(k+1)| \tag{4.7}$$

Where the $i_{\alpha}^*(k + 1)$ and $i_{\beta}^*(k + 1)$ will be the real and imaginary elements of the reference current. The $i_{\alpha}^p(k + 1)$ and $i_{\beta}^p(k + 1)$ will be the real and imaginary elements of the predicted load current. The reference current is assumed that it will not vary in one sampling period, therefore, the reference current in time $k + 1$ and k will be the same:

$$i(k + 1)^* = i(k)^* \tag{4.8}$$

The presumption will not affect the results of the frequency of sampling is fast. The control scheme of predictive current can be seen below 4.4

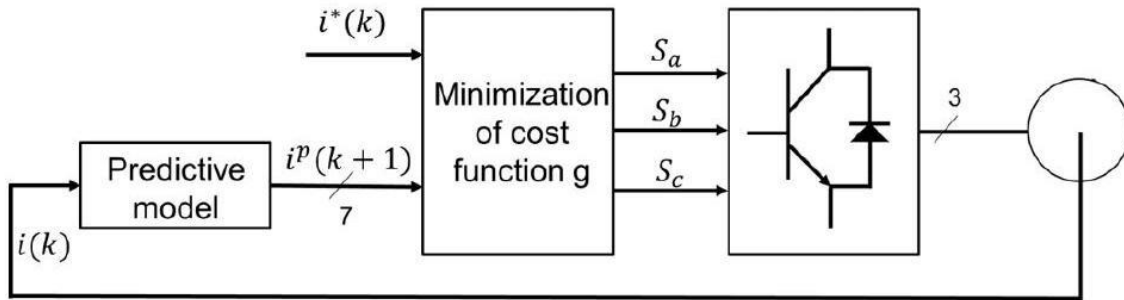


Figure 4.4: The control scheme of the model predictive current control

Similarly, the real current from the converter will enter the predictive model and obtain different predicted currents. If the three-phase, two-level converter is applied, seven different predicted currents will be obtained. Then, the reference current and the predicted current will be used to evaluate the cost function. The optimal current that minimizes the value of cost function is chosen to generate control signal. And finally, the control signal will be applied to the converter.

3.2.2 Model design

Converter model design: the three-phase, two-level power converter used to convert from DC to AC can be seen below 4.5 .

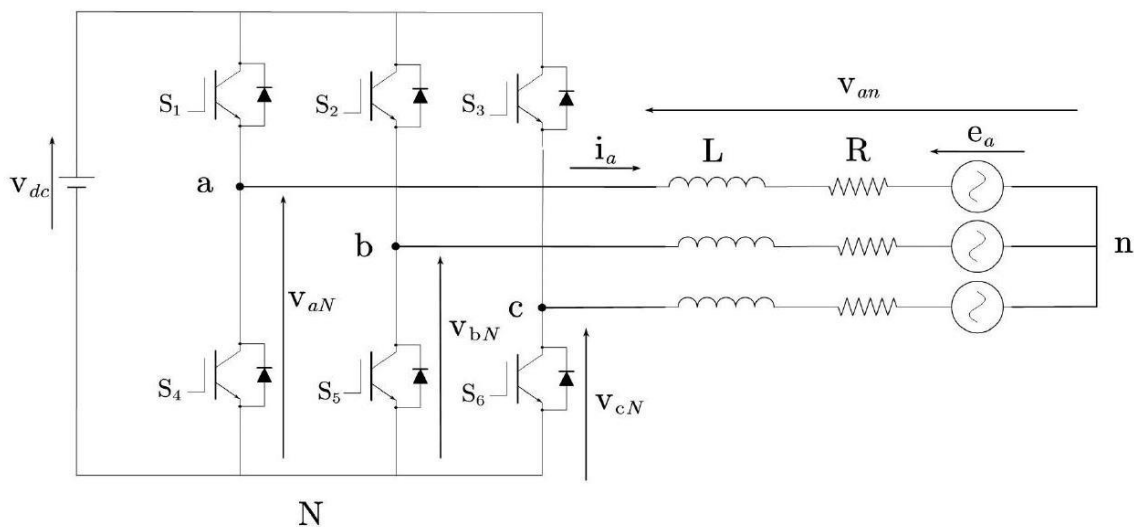


Figure 4.5: Voltage source converter circuit

Similar to the converter introduced in 2.17, there are eight different voltage vectors for different switching states.

Table 4: Different output voltage of 2 levels VSC in $\alpha\beta$ reference frame

S_{ag}	S_{bg}	S_{cg}	v_α	v_β	Vector
0	0	0	0	0	V_0
0	0	1	$-\frac{V_{bus}}{3}$	$-\frac{\sqrt{3}V_{bus}}{3}$	V_5
0	1	0	$-\frac{V_{bus}}{3}$	$\frac{\sqrt{3}V_{bus}}{3}$	V_3
0	1	1	$-\frac{2}{3}V_{bus}$	0	V_4
1	0	0	$\frac{2}{3}V_{bus}$	0	V_1
1	0	1	$-\frac{1}{3}V_{bus}$	$-\frac{\sqrt{3}V_{bus}}{3}$	V_6
1	1	0	$-\frac{1}{3}V_{bus}$	$\frac{\sqrt{3}V_{bus}}{3}$	V_2
1	1	1	0	0	V_7

An accurate converter model can be used to improve the switching frequencies, which considers the dead time, IGBT saturation voltage and forward voltage drop [8]. In this section, the simple model of the three-phase, two-level converter model will be applied.

Load model design: as can be seen in Figure 4.5 , the equations to describe the dynamics of the load currents can be calculated as:

$$v_{aN} = L \frac{di_a}{dt} + R * i_a + e_a + v_{nN} \tag{4.9}$$

$$v_{bN} = L \frac{di_b}{dt} + R * i_b + e_b + v_{nN} \tag{4.10}$$

$$v_{cN} = L \frac{di_c}{dt} + R * i_c + e_c + v_{nN} \tag{4.11}$$

Where R represents the resistance of the load and L represents the inductance of the load. The voltage vector can be calculated as:

$$v = \frac{2}{3}(v_{aN} + av_{bN} + a^2v_{cN}) \tag{4.12}$$

Substitute the equations 4.9,4.10,4.11 into the equation 4.12 , then:

$$v = \frac{L * d \left(\frac{2}{3}(i_a + ai_b + a^2i_c) \right)}{dt} + R \left(\frac{2}{3}(i_a + ai_b + a^2i_c) \right) + \frac{2}{3}(e_a + ae_b + a^2e_c) + \frac{2}{3}(v_{nN} + av_{nN} + a^2v_{nN})$$

Because the space vector of the load current and back-emf voltage are defined as follows:

$$i = \frac{2}{3} * (i_a + ai_b + a^2i_c) \tag{4.14}$$

$$e = \frac{2}{3} * (e_a + ae_b + a^2e_c) \tag{4.15}$$

Assume the last term of Equation 4.13 is 0 , then the voltage vector becomes:

$$v = Ri + L \frac{di}{dt} + e \tag{4.16}$$

Where v is the vector of voltage, which is generated using the converter. And i represents the current of the load. The back emf voltage is e, which is also assumed to be sinusoidal.

Discrete model design: because the equation of the load current derived in 4.16 needs the discretization process, this section will design the discrete model for prediction. The prediction model is applied to forecast the future load current. Because the system is the first-order system, forward Euler method will be used, which can be seen below:

$$\frac{di}{dt} \approx \frac{i(k + 1) - i(k)}{T_{\text{sampling}}} \tag{4.17}$$

According to the equation 4.16 the $\frac{di}{dt}$ can be expressed:

$$\frac{di}{dt} = \frac{v - Ri - e}{L} \tag{4.18}$$

Then, the predicted current $i^p(k + 1)$ will be:

$$i^p(k + 1) = i(k) - \frac{T_s R}{L} * i(k) + \frac{T_s}{L} (v(k) - \check{e}(k)) \tag{4.19}$$

Where $\check{e}(k)$ represents the estimated back-emf voltage. Using measured data of the load, the back-emf voltage is calculated by:

$$\check{e}(k - 1) = v(k - 1) - \frac{L * i(k)}{T_s} - \left(R * i(k - 1) - \frac{L}{T_s} * i(k - 1) \right) \tag{4.20}$$

Where $\check{e}(k - 1)$ is the estimation of $e(k - 1)$. For high sampling frequency, the back-emf voltage will not change during one sampling interval, then:

$$\check{e}(k) = \check{e}(k - 1) \tag{4.21}$$

Then, the estimated predicted current $i(k + 1)$ is obtained through measured current $i(k)$ and voltage $v(k)$.

3.2.3 Model predictive current control simulation

As mentioned in the section above, the converter model and load model have been designed. This section will explain the realization using the model predictive current control (MPCC) and simulation will also be conducted. The control scheme can be seen below 4.6

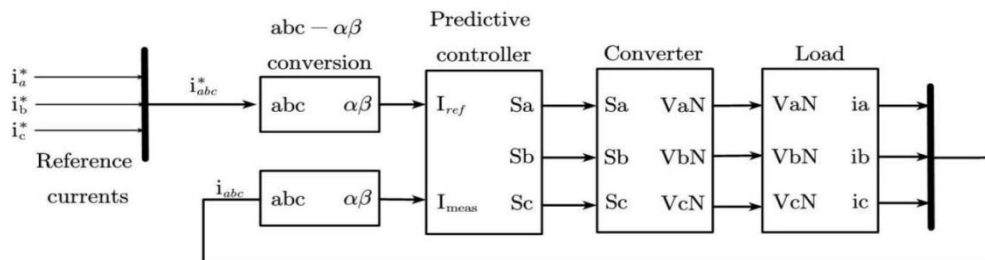


Figure 4.6: The scheme for model predictive current control of the converter

The reference currents and real currents will be first converted from abc frame to $\alpha\beta$ frame. Then, the controller will decide on the control signal to the converter. Then, the voltage created by the converter will be given to the load. And finally, the load model will generate the measured currents.

Because the simulation is conducted under the $\alpha\beta$ reference frame, the first step will be to achieve the transformation from the abc frame to $\alpha\beta$ frame. The currents in the stator reference frame are calculated by:

$$i_\alpha = \frac{2}{3} * \left(i_a - \frac{1}{2} * i_b - \frac{1}{2} * i_c \right) \tag{4.22}$$

$$i_\beta = \frac{2}{3} * \left(\frac{\sqrt{3}}{2} * i_b - \frac{\sqrt{3}}{2} * i_c \right) \tag{4.23}$$

Therefore, the realization of the transformation in Simulink can be seen below:

The three-phase converter voltage V_{aN} , V_{bN} and V_{cN} are expressed as:

$$V_{aN} = V_{dc} * S_a \tag{4.24}$$

$$V_{bN} = V_{dc} * S_b \tag{4.25}$$

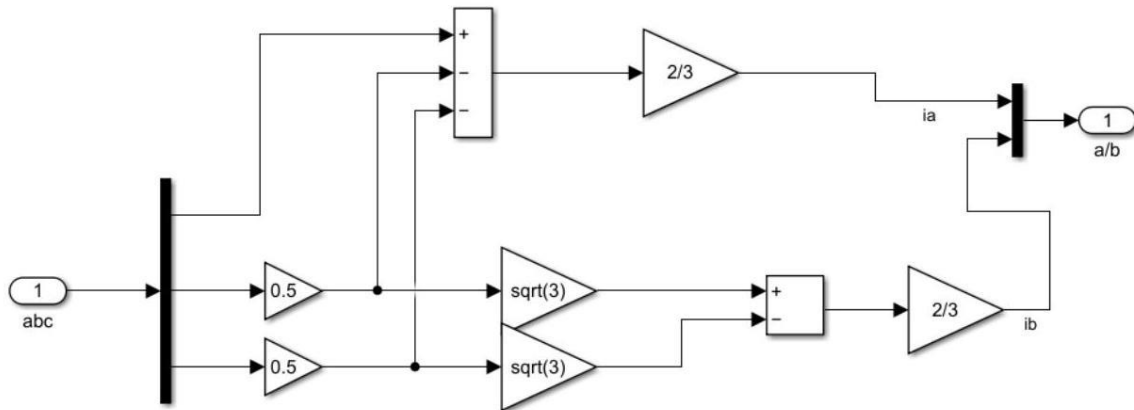


Figure 4.7: The realization of abc to $\alpha\beta$ transformation

$$V_{cN} = V_{dc} * S_c \tag{4.26}$$

The voltage of each leg to the negative busbar (N) can be obtained by multiplying DC bus voltage. Therefore, the Simulink model for the converter can be seen below 4.8 .

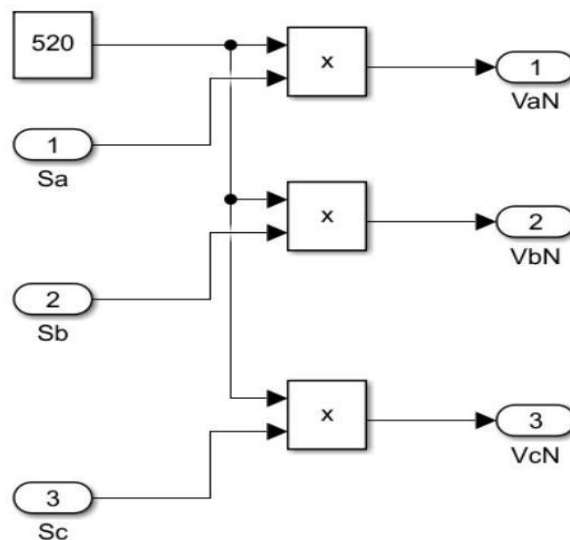


Figure 4.8: Simulink model for the converter

The value of V_{dc} is set to 520 V. The load voltages of the three phases can be seen below:

$$v_{an} = v_{aN} - v_{nN} \tag{4.27}$$

$$v_{bn} = v_{bN} - v_{nN} \tag{4.28}$$

$$v_{cn} = v_{cN} - v_{nN} \tag{4.29}$$

Substitute Equation 4.9,4.10,4.11 into 4.27,4.28,4.29 Then,

$$v_{aN} + v_{bN} + v_{cN} = \frac{d(i_a + i_b + i_c)}{dt} * L + R * (i_a + i_b + i_c) + (e_a + e_b + e_c) + 3 * v_{nN} \tag{4.30}$$

Because the addition of three phases' currents will be 0 and the addition of three back-emf voltage will be 0 . Then, the common mode voltage v_{nN} is calculated by:

$$v_{nN} = \frac{1}{3}(v_{aN} + v_{bN} + v_{cN}) \tag{4.31}$$

Then, the v_{an}, v_{bn}, v_{cn} can be obtained by:

$$v_{an} = L \frac{di_a}{dt} + Ri_a + e_a \tag{4.32}$$

$$v_{bn} = L \frac{di_b}{dt} + Ri_b + e_b \tag{4.33}$$

$$v_{cn} = L \frac{di_c}{dt} + Ri_c + e_c \tag{4.34}$$

Applying Laplace transform for Equations 4.32,4.33,4.34, then:

$$\frac{1}{Ls + R} = \frac{I_a}{V_{an} - E_a} \tag{4.35}$$

$$\frac{1}{Ls + R} = \frac{I_b}{V_{bn} - E_b} \tag{4.36}$$

$$\frac{1}{Ls + R} = \frac{I_c}{V_{cn} - E_c} \tag{4.37}$$

The back-emf is presumed to be the sinusoidal voltage with constant value and frequency. Therefore, the sine wave module in Simulink will be used to represent them. Then, the Simulink model for the load model can be seen below 4.9 .

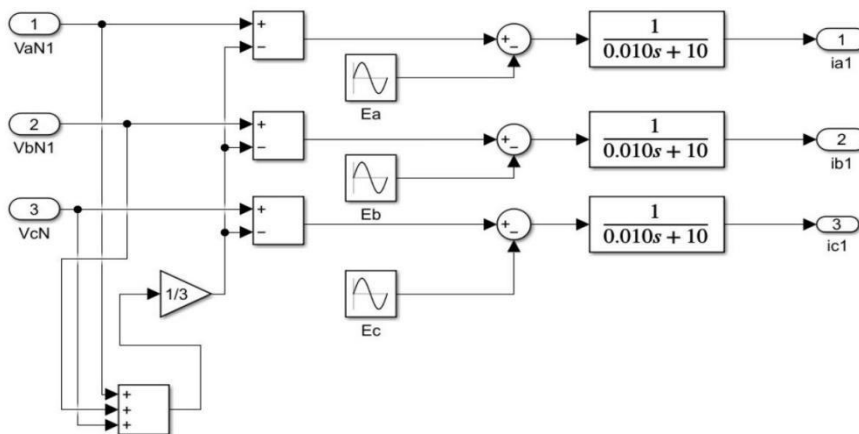


Figure 4.9: Simulink model for the load

In Simulink, the DC link voltage will be set to 520 V. The inductance and the resistance will be set to 10mH and 10Ω. The peak-to-peak voltage of back-emf will be set to 100 . The predictive controller is achieved by the MATLAB function.

The estimation of back-emf will be conducted first, and then the predicted current for every switching state will be calculated. The designed cost function is employed to compare the differences between the predicted current and the reference current. The optimal voltage vector that can minimize the cost function is chosen. And the process will repeat for the next sampling time. Therefore, the part of the code can be seen below:

Listing 1: The core code for model predictive control

```

% Estimation of back-emf
epeak = v(x_old) - L/Ts*i_k - (R - L/Ts)*i_old;

% Record measured current for the next cycle
i_old = i_k;
for i = 1:7

% Different voltage vectors for predicting current
v_o1 = v(i);

% Predict current at instant time k+1
i_k1 = (1 - R*T/L)*i_k + Ts/L*(v_o1 - epeak);

% Cost function design
g = abs(real(ik_ref - i_k1)) + abs(imag(ik_ref - i_k1));
    
```

63

```

% Select the best value
if (g < g_opt)
g_opt = g;
x_opt = i;
end
end
    
```

Where i_{old} is $i(k - 1)$, i_k is $i(k)$ and i_{k1} is $i(k + 1)$. After all the switching states are simulated, the optimal voltage vector will be chosen. The whole code for the controller can be seen in the appendix. Then, the whole design in Simulink can be seen below:

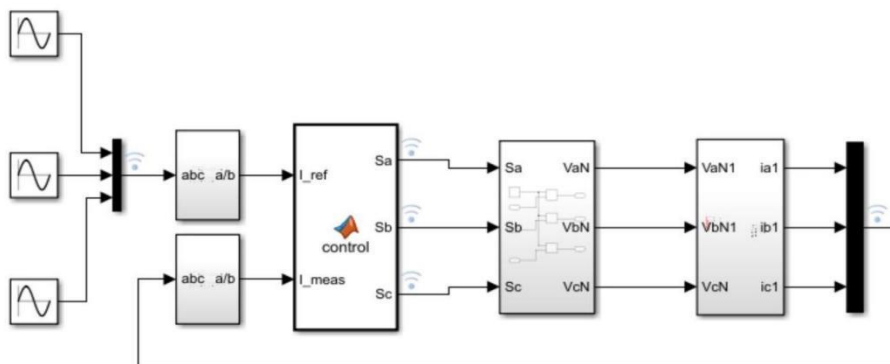


Figure 4.11: The design for the MPC for the converter

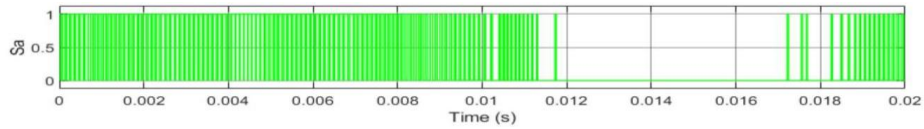
The design in Simulink 4.11 will be similar to the scheme designed before 4.6 The three reference currents will be represented by the three sine waves, which have the same frequency $50 * 2\pi Hz$ and the same amplitude 10A. But the difference between each phase will be 120 degrees. The simulation results for the three control signal S_a, S_b, S_c can be seen below 4.12 .

After obtaining the control signals, the generated voltage V_aN, V_bN, V_cN will be 4.13 .

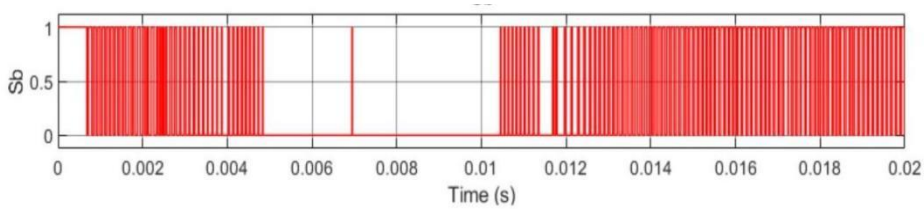
Because the DC voltage is set to 520 V, the voltage generated will be 520 V and 0 V at different times. Finally, the simulation results of the reference currents and measured currents can be seen below 4.14.

The simulation time is set from 0 s to 0.02 s because of the high frequency. The measured currents can track the reference currents very well and have fast dynamic behaviour and short response time. At 0.0005 s, the measured currents have already tracked the reference currents. This demonstrates that the objective of the control has been achieved.

Sa



Sb



Sc

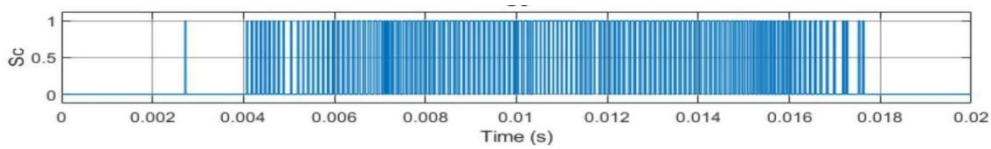


Figure 4.12: The control signals Sa, Sb, Sc

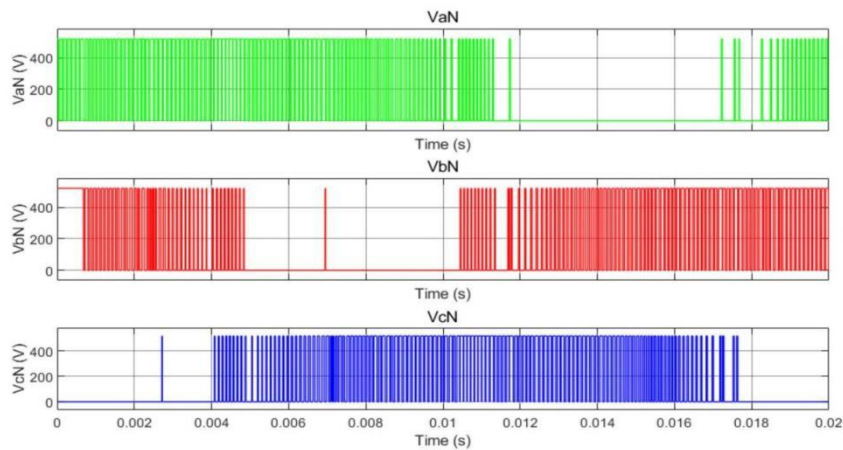


Figure 4.13: The generated voltage VaN, VbN, VcN

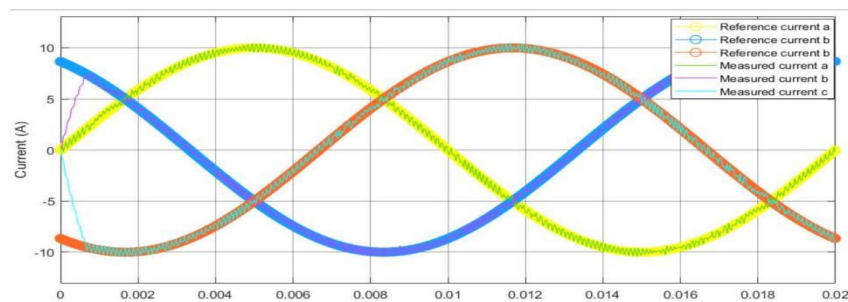


Figure 4.14: The simulation results for the measured currents and reference currents

3.3 Model predictive torque control of DFIG-based wind turbine

The voltage vector can adjust the flux of the stator and electromagnetic torque, which means that the model predictive control can also be used to modify the torque. Therefore, model predictive torque control is proposed, which is also a direct torque control. This means the dynamic behaviour will be good with no bandwidth limitation for the torque dynamics [43]. This section will first introduce the theory of model predictive torque control of the wind turbine and obtain a control scheme for it. Finally, the simulation results will be also presented.

3.3.1 The theory of model predictive torque control

Before designing the control method of the induction machine, the dynamic model of the DFIG-WT needs to be known. Similarly, the model can be obtained under the abc reference frame. However, the three variables make the process of mathematical deriving become difficult. Because the three axes are dependent linearly, two variables are enough to describe the physical behaviours. Therefore, the dynamic model rotating at angular frequency ω_k can be seen below:

$$v_s = R_s i_s + \frac{d\phi_s}{dt} + j\omega_k \phi_s \quad (4.38)$$

$$v_r = R_r i_r + \frac{d\phi_r}{dt} + j(\omega_k - \omega)\phi_r \quad (4.39)$$

$$\phi_s = L_s i_s + L_m i_r \quad (4.40)$$

$$\phi_r = L_m i_s + L_r i_r \quad (4.41)$$

Where ω means the rotor angular speed. And the torque is expressed as:

$$T = \frac{3}{2} p \text{Re} \{ \bar{\phi}_s i_s \} \quad (4.42)$$

Where p represents the number of the pair of the pole. And $\bar{\phi}$ represents the conjugate value of the flux. The torque will affect rotor speed ω_m . The dependency between the torque and the rotor speed is shown below:

$$J \frac{d\omega_m}{dt} = T - T_{load} \quad (4.43)$$

Where J represents the moment of inertia, T_{load} as the load torque, the mechanical rotor speed is ω_m . The relation between the mechanical rotor speed and electric rotor speed is:

$$\omega = p\omega_m \quad (4.44)$$

To apply the control strategy in the model, the state variables need to be chosen. In this project, the stator current and rotor flux will be chosen as the state variables. The reason for choosing the stator current is that it can be measured and the unnecessary parameters can be ignored, such as back-emf voltage, and stator resistance. The current of the stator and the flux of the rotor are calculated by:

$$i_s + \tau_\sigma * \frac{di_s}{dt} = -j * \omega_k \tau_\sigma i_s + \frac{k_r}{R_\sigma} * \left(\frac{1}{\tau_r} - j * \omega \right) \phi_r + \frac{v_s}{R_\sigma} \quad (4.45)$$

$$\phi_r + \tau_r * \frac{d\phi_r}{dt} = -j * (\omega_k - \omega) \tau_r \phi_r + L_m i_s \quad (4.46)$$

where

$$\begin{aligned} \tau_s &= \frac{L_s}{R_s} \\ \tau_r &= \frac{L_r}{R_r} \\ \sigma &= 1 - \frac{L_m^2}{L_s L_r} \\ k_r &= \frac{L_m}{L_r} \\ k_s &= \frac{L_m}{L_s} \\ R_\sigma &= R_s + R_r k_r^2 \\ \tau_\sigma &= \frac{\sigma L_s}{R_\sigma} \end{aligned}$$

The estimation of the flux of the rotor and stator will use the above equations. Compared with traditional direct torque control (DTC), model predictive torque control (MPTC) will calculate the future flux and torque of the stator. Therefore, the designed cost function will consider both the stator flux and the torque. This means the complex constraints in the industry can be handled by the MPTC. And there will be a weight factor between stator flux and torque. Similarly, the model predictive torque control will select the optimal voltage vector that can minimize the designed cost function value at every sampling time. Therefore, the control scheme of model predictive torque control is shown below 4.15 .

The stator and rotor flux estimation module will be used to obtain the estimation of $\hat{\phi}_r(k)$ and $\hat{\phi}_s(k)$ using the currents. Then, the predicted torque $T(k + 1)$ and $\phi_s(k + 1)$ will be forecast using the estimations in the torque and flux prediction module. Finally, the predicted torque and stator flux will be employed to evaluate the designed cost function. The optimal voltage vector that minimizes the value of the cost function is used to create the control signal. Then, the control signal will control the converter. In the project, the 3-phase, 2-level converter will be implemented. The voltage vector for each switching state can be seen in the previous section. The speed controller will use the difference between the reference ω^* and ω to obtain the reference torque T_* .

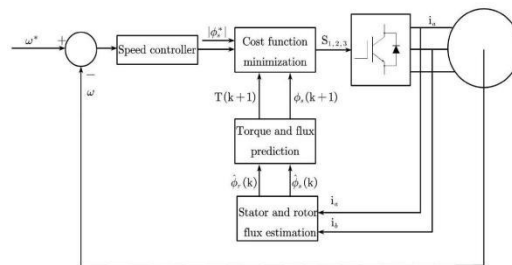


Figure 4.15: The scheme for model predictive torque control

Therefore, the stator and rotor flux estimation ϕ_s and ϕ_r need to be derived firstly. The stator voltage can be calculated as:

$$v_s = R_s i_s + \frac{d\phi_s}{dt} \tag{4.47}$$

Because the system is a first-order system, the Euler method will be also used, therefore, the estimation of stator flux will be:

$$\hat{\phi}_s(\hat{k}) = \hat{\phi}_s(k - 1) + T_s v_s(k) - R_s T_s i_s(k) \tag{4.48}$$

Because the stator flux can be obtained as:

$$\phi_s = i_s L_s + i_r L_m \tag{4.49}$$

And the rotor flux is:

$$\phi_r = i_s L_m + i_r L_r \quad (4.50)$$

Then, the flux of the rotor can be calculated as:

$$\hat{\phi}_r = \frac{L_r}{L_m} * \hat{\phi}_s + i_s \left(L_m - \frac{L_r L_s}{L_m} \right) \quad (4.51)$$

After discretizing the equation 4.51 , the estimation of rotor flux will be:

$$\hat{\phi}_r(k) = \frac{L_r}{L_m} \hat{\phi}_s(k) + i_s(k) \left(L_m - \frac{L_r L_s}{L_m} \right) \quad (4.52)$$

Because the flux and torque of stator are selected as the controlled variables, the predicted stator flux in the next sampling time $k + 1$ will be:

$$\phi_s^p(k + 1) = \hat{\phi}_s(k) + T_s v_s(k) - R_s T_s i_s(k) \quad (4.53)$$

The predicted stator flux is generated by approximating the derivative of the flux of the stator. Because the electromagnetic torque can be calculated by:

$$T = \frac{3}{2} p \text{Im} \{ \bar{\phi}_s i_s \} \quad (4.54)$$

Substitute the Equation 4.53 into Equation 4.54 , then:

$$T^p(k + 1) = \frac{3}{2} * p * \text{Im} \{ \bar{\phi}_s^p(k + 1) i_s^p(k + 1) \} \quad (4.55)$$

Therefore, the predicted stator current is needed, which can be obtained from Equation 4.45

$$i_s^p(k + 1) = \left(i_s(k) + \frac{T_s}{\tau_\sigma} i_s(k) + \frac{T_s}{(\tau_\sigma + T_s) R_\sigma} * \left[\frac{k_r \hat{\phi}_r(k)}{\tau_r} - k_r j \omega \hat{\phi}_r(k) + v_s(k) \right] \right) \quad (4.56)$$

As shown in the equations above, the predicted stator flux and the torque will be expressed as the voltage vector $v_s(k)$. Therefore, there will be seven different predicted stator flux and torque according to different voltage vectors if the three-phase converter is employed. And the cost function will rely on the flux and torque of the stator, which is expressed as:

$$g = |T^* - T^p(k + 1)| + \lambda_\phi |\phi_s^* - \phi_s^p(k + 1)| \quad (4.57)$$

Where λ_ϕ represents the weight factor, which will decide the relative importance of the flux. Normally, the weight factor can be calculated by the equation

$$\lambda_\phi = \frac{T_n}{|\phi_{sn}|} \quad (4.58)$$

Where the T_n and $|\phi_{sn}|$ is the nominal value of the torque and stator flux.

3.3.2 Simulation results

After explaining the working principles of model predictive torque control strategy, the realization of the control will be implemented in Simulink. In this simulation, the three-phase, two-level converter is employed. Specially, the speed controller will be designed to obtain the reference torque. The whole control Simulink model for model predictive torque control can be seen below 4.16

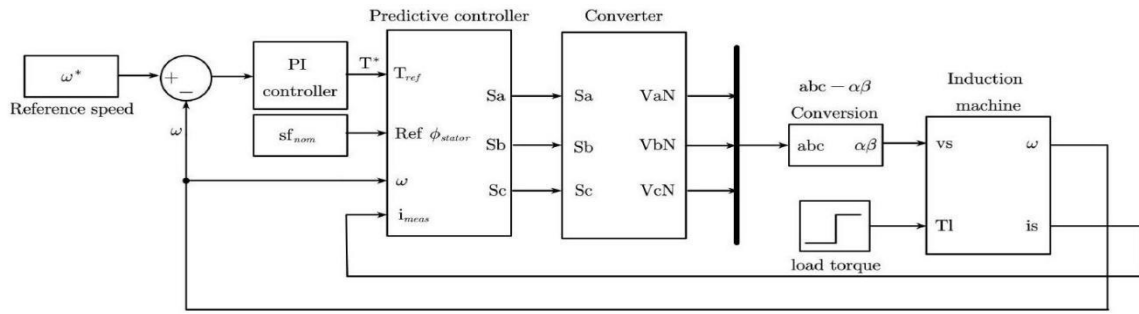


Figure 4.16: The Simulink model for model predictive

The designed PI controller is applied as the controller of speed to create the reference torque by the error between the reference speed and the real speed. The reference stator flux is nominal stator flux. Then, the designed predictive controller will generate control signals to the voltage source converter. The induction machine will use the voltage of the stator and the torque of the load to generate the angular speed and stator current. And the generated stator current will enter the designed predictive controller. Therefore, the speed controller will be first constructed. To track the reference speed, the PI controller will receive the error between the reference speed and the real speed. Because the transfer function between the torque and the speed is:

$$\frac{\omega(s)}{T(s)} = \frac{1}{Js} \tag{4.59}$$

The saturation will be used to limit the amplitude of the torque. In this project, the value of k_p is set to 100 and the k_i is set to 2000. The upper limit output is 30 and the lower limit output is set to -30. The PI speed controller in Simulink can be seen in 4.17.

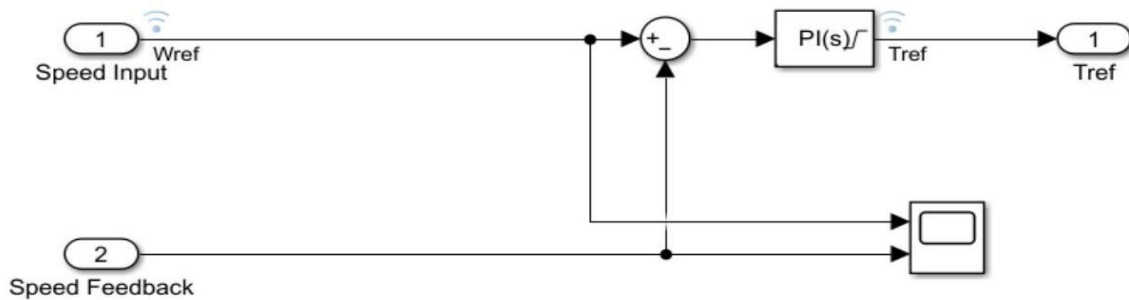


Figure 4.17: The speed controller in Simulink

The simulation results can be seen below 4.18 :

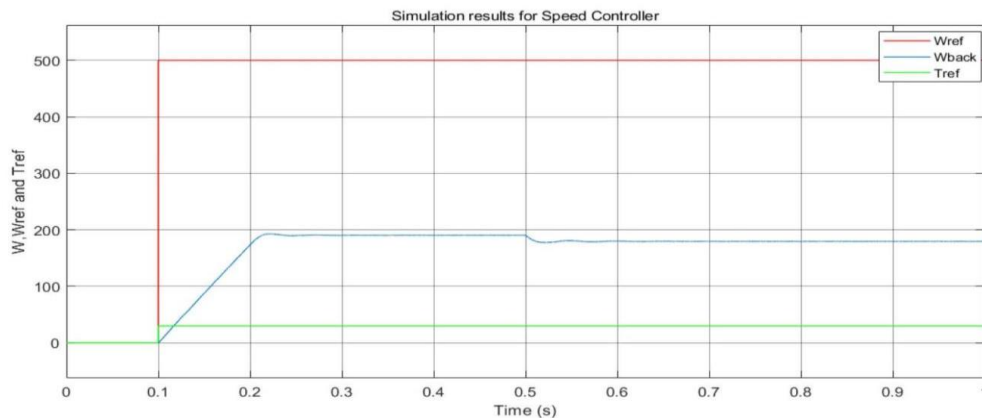


Figure 4.18: The simulation results for the speed controller

In this project, the weight factor for the torque is 1.25 and the weight factor for the flux is 5 . These weight factors can be changed for different control requirements. Similarly, the converter will use the dc voltage and three control signals, which can be seen below 4.19 .

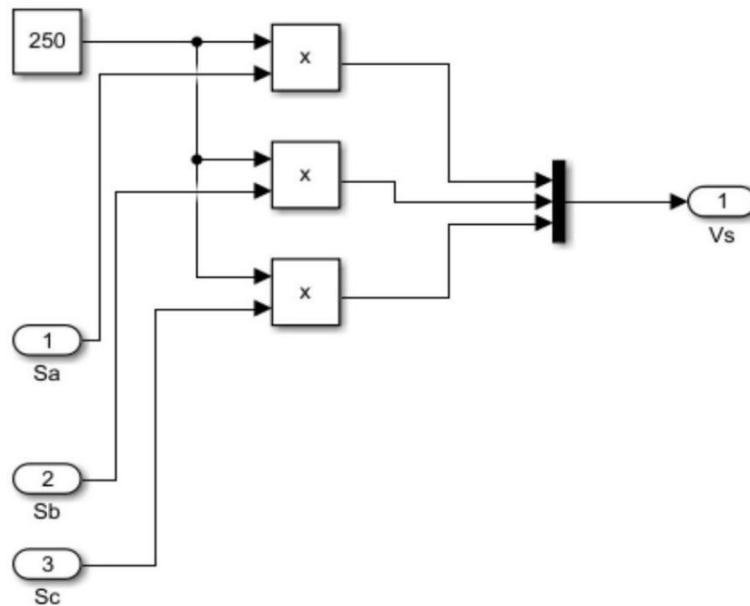


Figure 4.19: The Simulink model for the converter

The value of the dc voltage is set to 250 V. The Simulink model of the conversion between the abc reference frame and $\alpha\beta$ frame has been presented in the previous section. And the induction machine dynamic model in Simulink can be seen below 4.20 .

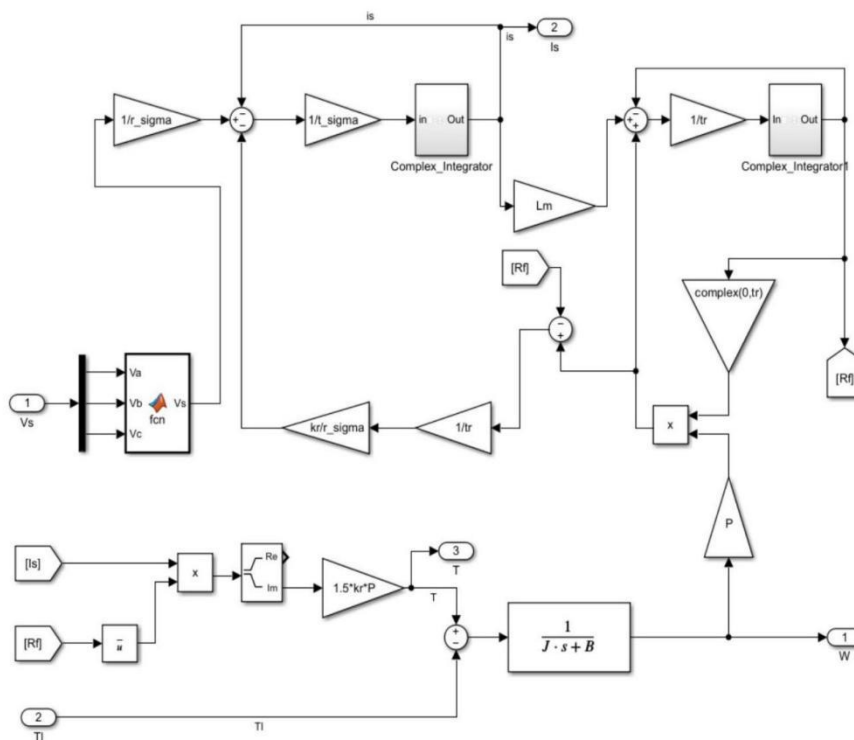


Figure 4.20: The Simulink model for the induction machine

The load torque and the stator voltage will be used as the inputs and the torque, rotor speed and stator current will be used as the outputs. In this model, the conversion between the abc and $\alpha\beta$ frame is conducted first. Then, the

dynamics of the stator and rotor 4.45,4.46 will be achieved. In the process, the complex integrator module will be used in the induction machine, which can be seen below:

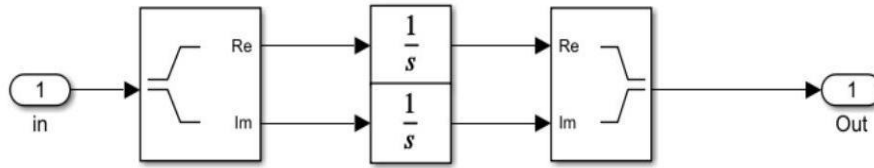


Figure 4.21: The complex integrator model

There are two complex integrators for the state variables i_s and ϕ_r . Especially, the complex integrator can integrate the real and imaginary elements separately. Finally, the torque needs to be calculated, which can be calculated as:

$$T = \frac{3}{2}p\text{Im}\{\bar{\phi}_r i_s\} \tag{4.60}$$

In the simulation, the torque is obtained by the rotor flux and the stator current. Because the mechanical equation for the rotor is:

$$\frac{d\omega}{dt} = \frac{T - T_{load}}{J} \tag{4.61}$$

Therefore, the rotor speed will be calculated by the electromagnetic torque and load torque disturbance T_{load} . After multiplying the number of the pairs of poles, the rotor speed ω is obtained. The value of the parameters for the induction machine is presented in the appendix.

The simulation time is set from 0 to 1 s. The reference speed is replaced by a step module in Simulink. The step time is 0.1 s and the speed will change from 0 to 500(rad/s). The nominal stator flux is chosen to 0.4 Wb. And the load torque disturbance is also replaced by the step module. The step time is set to 0.5 s and the value will change from 0 to 20Nm. The simulation results for the corresponding stator currents can be seen below 4.22 .

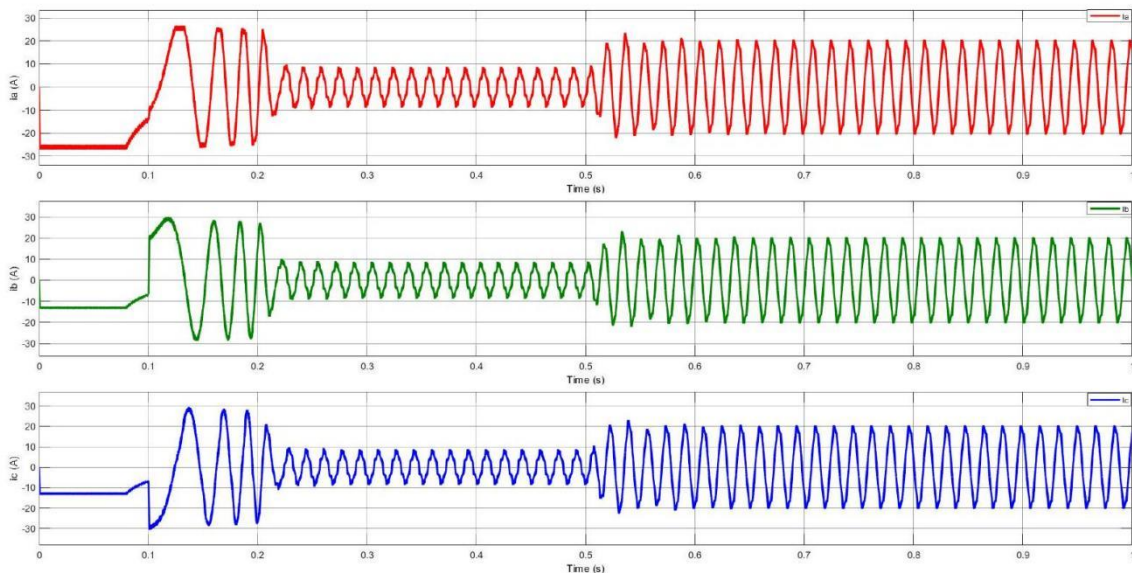


Figure 4.22: The simulation results for the stator currents

When the reference speed changes, the currents will also change with fast response time at 0.5 s. And the currents quickly change back to the steady state after the changes in speed at 0.1 s and the load torque disturbance at 0.5 s. Additionally, the torque control results can be seen below:

The torque can track the reference torque very fast at time 0.1 s when the speed increase. When the speed remains at 180rad/s after 0.2 s, the torque will decrease to 0 because there is no difference in speed. When the load torque increase, the torque will also increase with fast dynamic and short response time. This is because the model predictive torque control (MPTC) is a kind of direct control without the PI controller. Therefore, there will be no limitation of bandwidth for the dynamics of the torque. In addition, low harmonic distortion is achieved, which is also the advantage of model predictive torque control.

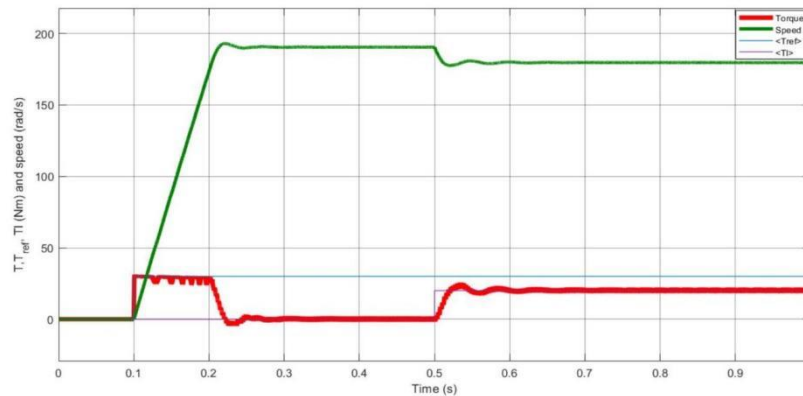


Figure 4.23: The simulation results for the torque control

4 Conclusion

In conclusion, this paper provides a comprehensive analysis of advanced control strategies for doubly-fed induction generator-based wind turbines (DFIG-WT), focusing on the transition from vector control to model predictive control (MPC). The study begins by outlining the structural and operational aspects of DFIG-WT, emphasizing the limitations of vector control in handling dynamic constraints. It then demonstrates the effectiveness of MPC in enhancing DFIG-WT performance, particularly through fast current reference tracking and robust torque management. The application of MPC in current control for three-phase two-level converters and predictive torque control illustrates its superior capability in adapting to varying operational conditions. Overall, the research concludes that MPC offers significant improvements in the accuracy and responsiveness of DFIG-WT control systems, thereby optimizing wind energy transformation and contributing to more efficient and reliable wind power generation.

References

- [1] D. Y. Leung and Y. Yang, "Wind energy development and its environmental impact: A review," *Renewable and Sustainable Energy Reviews*, vol. 16, no. 1, pp. 1031-1039, 2012. [Online]. Available: <https://www.sciencedirect.com/science/article/pii/S1364032111004746>
- [2] R. Tiwari and N. R. Babu, "Recent developments of control strategies for wind energy conversion system," *Renewable and Sustainable Energy Reviews*, vol. 66, pp. 268-285, 2016. [Online]. Available: <https://www.sciencedirect.com/science/article/pii/S1364032116304221>
- [3] J. Rodriguez and P. Cortes, *Introduction*, 2012, pp. 1-16.
- [4] I. Ngamroo, "Review of dfig wind turbine impact on power system dynamic performances," *IEEJ Transactions on electrical and electronic engineering*, vol. 12, no. 3, pp. 301-311, 2017.
- [5] G. Abad, J. López, M. Rodríguez, L. Marroyo, and G. Iwanski, *Introduction to A Wind Energy Generation System*, 2011, pp. 1-85.
- [6] J. Rodriguez and P. Cortes, *Classical Control Methods for Power Converters and Drives*, 2012, pp. 17 – 30.
- [7] A. Linder, R. Kanchan, P. Stolze, and R. Kennel, *Model-based predictive control of electric drives*. Cuvillier Verlag, 2010.
- [8] J. Rodriguez and P. Cortes, *Model Predictive Control*, 2012, pp. 31-39.
- [9] S. Sahoo, B. Subudhi, and G. Panda, "Comparison of output power control performance of wind turbine using pi, fuzzy logic and model predictive controllers," *International Journal of Renewable Energy Research*, vol. 8, no. 2, pp. 1062-1070, 2018.

- [10] K. M. Passino, S. Yurkovich, and M. Reinfrank, *Fuzzy control*. Addison-wesley Reading, MA, 1998, vol. 42.
- [11] J. P. da Costa, H. Pinheiro, T. Degner, and G. Arnold, "Robust controller for dfigs of grid-connected wind turbines," *IEEE Transactions on Industrial Electronics*, vol. 58, no. 9, pp. 4023-4038, 2011.
- [12] M. I. Martinez, G. Tapia, A. Susperregui, and H. Camblong, "Sliding-mode control for dig rotor-and grid-side converters under unbalanced and harmonically distorted grid voltage," *IEEE Transactions on Energy Conversion*, vol. 27, no. 2, pp. 328-339, 2012.
- [13] S. Li, T. A. Haskew, K. A. Williams, and R. P. Swatloski, "Control of dfig wind turbine with directcurrent vector control configuration," *IEEE Transactions on Sustainable Energy*, vol. 3, no. 1, pp. 1 – 11, 2012.
- [14] M. Popescu, *Induction motor modelling for vector control purposes*. Helsinki University of Technology Espoo, Finland, 2000.
- [15] R. de Doncker and D. Novotny, "The universal field oriented controller," in *Conference Record of the 1988 IEEE Industry Applications Society Annual Meeting*, 1988, pp. 450-456 vol. 1.
- [16] R. W. De Doncker, F. Profumo, M. Pastorelli, and P. Ferraris, "Comparison of universal field oriented (ufo) controllers in different reference frames," *IEEE transactions on Power Electronics*, vol. 10, no. 2, pp. 205-213, 1995.
- [17] L. Xu and W. Cheng, "Torque and reactive power control of a doubly fed induction machine by position sensorless scheme," *IEEE Transactions on Industry Applications*, vol. 31, no. 3, pp. 636-642, 1995.
- [18] S. Wang and Y. Ding, "Stability analysis of field oriented doubly-fed induction machine drive based on computer simulation," *Electric Machines and power systems*, vol. 21, no. 1, pp. 11-24, 1993.
- [19] B. Hopfensperger, D. Atkinson, and R. Lakin, "Stator flux oriented control of a cascaded doubly-fed induction machine," *IEE Proceedings-Electric Power Applications*, vol. 146, no. 6, pp. 597-605, 1999.
- [20] G. Abad, J. López, M. Rodríguez, L. Marroyo, and G. Iwanski, *Vector Control Strategies for Grid-Connected DFIM Wind Turbines*, 2011, pp. 303-361.
- [21] V. Kaura and V. Blasko, "Operation of a phase locked loop system under distorted utility conditions," *IEEE Transactions on Industry Applications*, vol. 33, no. 1, pp. 58-63, 1997.
- [22] A. Perdana, O. Carlson, and J. Persson, "Dynamic response of grid-connected wind turbine with doubly fed induction generator during disturbances," in *Nordic workshop on power and industrial electronics*, vol. 1, no. 1. Citeseer, 2004, pp. 1-7.
- [23] J. B. Ekanayake, L. Holdsworth, X. Wu, and N. Jenkins, "Dynamic modeling of doubly fed induction generator wind turbines," *IEEE transactions on power systems*, vol. 18, no. 2, pp. 803-809, 2003.
- [24] L. Congwei, W. Haiqing, S. Xudong, and L. Fahai, "Research of stability of double fed induction motor vector control system," in *ICEMS'2001. Proceedings of the Fifth International Conference on Electrical Machines and Systems (IEEE Cat. No.01EX501)*, vol. 2, 2001, pp. 1203-1206 vol.2.
- [25] A. Petersson, L. Harnefors, and T. Thiringer, "Comparison between stator-flux and grid-fluxoriented rotor current control of doubly-fed induction generators," in *2004 IEEE 35th Annual Power Electronics Specialists Conference (IEEE Cat. No. 04CH37551)*, vol. 1. IEEE, 2004, pp. 482-486.
- [26] O. Kukrer, "Deadbeat control of a three-phase inverter with an output lc filter," *IEEE Transactions on Power Electronics*, vol. 11, no. 1, pp. 16-23, 1996.
- [27] K. Antoniewicz and M. Jasinski, "Experimental comparison of hysteresis based control and finite control state set model predictive control of shunt active power filter," in *2015 Selected Problems of Electrical Engineering and Electronics (WZEE)*. IEEE, 2015, pp. 1-6.
- [28] A. A. Julius, "Trajectory-based controller design for hybrid systems with affine continuous dynamics," in *2010 IEEE International Conference on Automation Science and Engineering*, 2010, pp. 1007 – 1012.
- [29] S. Kouro, P. Cortes, R. Vargas, U. Ammann, and J. Rodriguez, "Model predictive control-a simple and powerful method to control power converters," *IEEE Transactions on Industrial Electronics*, vol. 56, no. 6, pp. 1826-1838, 2009.
- [30] L. Wang, S. Chai, D. Yoo, L. Gan, and K. Ng, *Continuous-time Model Predictive Control (CMPC) of Electrical Drives and Power Converter*, 2015, pp. 285-313.
- [31] D. Y. L. Wang, S. Chai and K. Ng, *FCS Predictive Control in Reference Frame*, 2015, pp. 237-263.
- [32] S. Dixon and C. Hall, "Chapter 10 - wind turbines," in *Fluid Mechanics and Thermodynamics of Turbomachinery (Sixth Edition)*, sixth edition ed., S. Dixon and C. Hall, Eds. Boston: Butterworth-

- Heinemann, 2010, pp. 357-413. [Online]. Available: <https://www.sciencedirect.com/science/article/pii/B9781856177931000109>
- [33] M. Loucif, A. Boumediene, and A. Mechernene, "Backstepping control of double fed induction generator driven by wind turbine," in 3rd international conference on systems and control. IEEE, 2013, pp. 153-158.
- [34] R. Tariq Ahmedhamdi and M. Abdul Hussein, "Modeling and simulation of wind turbine generator using matlab-simulink," Journal of Al-Rafidain University College, vol. 40, pp. 282-300, 012017.
- [35] O. Apata and D. Oyedokun, "An overview of control techniques for wind turbine systems," Scientific African, vol. 10, p. e00566, 2020. [Online]. Available: <https://www.sciencedirect.com/science/article/pii/S2468227620303045>
- [36] M. Abdullah, A. Yatim, C. Tan, and R. Saidur, "A review of maximum power point tracking algorithms for wind energy systems," Renewable and Sustainable Energy Reviews, vol. 16, no. 5, pp. 3220-3227, 2012. [Online]. Available: <https://www.sciencedirect.com/science/article/pii/S1364032112001098>
- [37] G. Abad, J. López, M. Rodríguez, L. Marroyo, and G. Iwanski, Dynamic Modeling of the Doubly Fed Induction Machine, 2011, pp. 209-239.
- [38] G. Abad, J. López, M. Rodríguez, L. Marroyo and G. Iwanski, Appendix of Doubly Fed Induction Machine: Modeling and Control for Wind Energy Generation Applications, 2011, pp. 603-618.
- [39] G. Abad, J. López, M. Rodríguez, L. Marroyo, and G. Iwanski, Back-to-Back Power Electronic Converter, 2011, pp. 87-154.
- [40] H. Abu-Rub, M. Malinowski, and K. Al-Haddad, Properties and Control of a Doubly Fed Induction Machine, 2014, pp. 270-318.
- [41] L. Xu and P. Cartwright, "Direct active and reactive power control of dfig for wind energy generation," IEEE Transactions on Energy Conversion, vol. 21, no. 3, pp. 750-758, 2006.
- [42] E. F. Camacho and C. Bordons, Introduction to Model Based Predictive Control. London: Springer London, 1999, pp. 1-11. [Online]. Available: https://doi.org/10.1007/978-1-4471-3398-8_1
- [43] J. Rodriguez and P. Cortes, Predictive Control of Induction Machines, 2012, pp. 115-132.
- [44] I. Ngamroo, "Review of dfig wind turbine impact on power system dynamic performances," IEEJ Transactions on electrical and electronic engineering, vol. 12, no. 3, pp. 301-311, 2017.
- [45] R. Zavadil, N. Miller, A. Ellis, and E. Muljadi, "Making connections [wind generation facilities]," IEEE Power and Energy Magazine, vol. 3, no. 6, pp. 26-37, 2005.
- [46] S. Muller, M. Deicke, and R. De Doncker, "Doubly fed induction generator systems for wind turbines," IEEE Industry Applications Magazine, vol. 8, no. 3, pp. 26-33, 2002.
- [47] J. Rodriguez and P. Cortes, Predictive Control of a Three-Phase Inverter, 2012, pp. 41-63.